Understanding Spatial and Temporal Evolution of Progressive Excavation Damage Zone in Granitic Rocks – Development of a Novel Mine-by and Laboratory Experimental Framework at the BedrettoLab

List of Authors: Pooya Hamdi[1], Jonas Dickmann[1], Michal Kruszewski[1], Antonio Pio Rinaldi[2], Linus Villiger[2], Alexis Shakas[3], Mathew Perras[4], Navid Bahrani[5], Patrick Bianchi[2], Peter Achtziger-Zupančič[6], Steven Gaines[7], Kai Bröker[8], Xiaodong Ma[9], Paul A Selvadurai[3], Virginie Durand[10], Kavan Khaledi[6], Mohammadreza Jalali[1], Yousef Golabchi[11], Sam Harris[4], Alba Zappone[3], Mathilde Wimez[3], Marian Hertrich[3], Stefan Wiemer[2], Florian Amann[1,6]

Corresponding author: Pooya Hamdi, email: hamdi@lih.rwth-aachen.de

[1] Chair of Engineering Geology & Hydrogeology, RWTH Aachen University, Aachen, Germany
[2] Swiss Seismological Service, ETH Zurich, Zurich, Switzerland
[3] Department of Earth Sciences, ETH Zurich, Sonneggstrasse 5, Zurich, 8092, Switzerland
[4] Trent School of the Environment, Trent University, Peterborough, Ontario, Canada
[5] Department of Civil and Resource Engineering, Dalhousie University, Canada
[6] Fraunhofer Research Institution for Energy Infrastructures and Geotechnologies, IEG, Aachen, Germany
[7] Natural Resources Canada, Ontario, Canada
[8] Center for Hydrogeology and Geothermics, University of Neuchâtel, Neuchâtel, Switzerland.
[9] University of Science and Technology of China, School of Earth and Space Sciences, Hefei, China
[10] Geoazur Laboratory, Valbonne, France
[11] Department of Civil Engineering, Lassonde School of Engineering, York University, Canada

Abstract

Brittle damage around tunnels in the form of spalling is common in massive crystalline rocks subjected to high in-situ stresses. Understanding the short-term development and long-term evolution of the Excavation Damage Zone (EDZ) is particularly important for deep geological repositories (DGRs) for heat-generating nuclear waste, as the EDZ may provide preferential pathways for radionuclide migration. This paper presents an overview of the PRECODE mine-by experiment at BedrettoLab, a newly developed underground research laboratory (URL) in southern Switzerland designed to investigate brittle fracturing and EDZ evolution in crystalline rocks under repository-relevant conditions. The PRECODE tunnel was excavated in Rotondo Granite using both controlled drill-and-blast (D&B) and line-drilling and rock-breaking (LDRB) methods to evaluate the influence of excavation technique on EDZ characteristics. The experiment combines multidisciplinary in-situ monitoring including acoustic emission, distributed acoustic and strain sensing, hydraulic monitoring, electrical resistivity tomography, and terrestrial laser scanning with laboratory-based fracture mechanics and time-dependent testing under varying environmental conditions. The main objectives are to characterize short-term EDZ formation, investigate long-term crack growth and stress corrosion processes, quantify permeability evolution, and assess the interaction between excavation-induced damage and nearby fault zones. Preliminary results indicate clear differences in AE activity and EDZ development between excavation methods, while observations from the mature EDZ of the more than 40-year-old Bedretto Tunnel suggest ongoing time-dependent brittle fracturing. The coupled in-situ and laboratory datasets provide a unique basis for improving predictive models and long-term safety assessments for nuclear waste repositories in crystalline rocks.

1. Introduction

The brittle damage in the form of spalling and rock bursting is common in massive rocks under high stress conditions (Martin et al., 1997; Diederichs, 2007; Kaiser et al., 2010; Perras & Diederichs, 2016). Spalling is the development of visible extension fractures under a compressive stress regime that may or may not be violent (Diederichs, 2007). Strain bursting, in contrast, refers to the violent rupture of a rock volume under high stress levels, during which rock fragments of

varying sizes are ejected from the tunnel wall at high velocity, releasing stored energy (Kaiser et al., 1996). Understanding the shape, extent and properties of the Excavation Damage Zone (EDZ), and its evolution over time is of foremost relevance for safety analysis of underground infrastructures, particularly deep geological repositories for nuclear waste disposal. Within the EDZ, permeability is often increased (Kelsall et al., 1984; Rutqvist et al., 2009) and may provide preferred and interconnected flow pathways for the migration of radionuclides. In contrast to clayshales and salt rocks, crystalline rocks do not possess natural self-sealing or self-healing properties (Tsang et al., 2005; Bossart et al., 2017), and damage in the form of brittle fracturing tends to persist and may propagate over time under unfavorable conditions.

In-situ observations around tunnels in massive, brittle rocks have revealed that the stress-induced fracturing begins at stress levels well below the rock's laboratory unconfined compressive strength (Martin & Chandler, 1994; Martin, 1997; Diederichs, 2003; Diederichs et al., 2010). The stress level at which brittle fracturing is initiated around tunnels in the short-term (i.e. during the construction) has been found to be 35-50% of the rock strength determined at the laboratory scale (Martin et al., 1997). This stress level coincides with the crack initiation (CI) damage threshold that can be determined from laboratory samples using non-destructive methods such as strain measurement or acoustic emission monitoring (Eberhardt et al., 1999; Diederichs, 2003; Amann et al., 2011; Perras et al., 2024). In the near-field of a tunnel, where the confining stress is low, macroscopic and interconnected fractures may form, as the differential stress exceeds CI. The macroscopic fracture zone is limited in depth by the spalling limit that represents the boundary between extensional type failure and shear-dominated failure, and is defined by the ratio between the maximum and minimum principal stresses.

A variety of empirical and fracture mechanics studies (i.e. (Hoek, 1968; Diederichs, 2007; Kaiser & Kim, 2008) on crystalline rocks showed that the spalling limit ranges between σ_1/σ_3=1/20-1/15. For confining stresses beyond the spalling limit, the rock fails in shear. While this rock mechanical concept for the short-term formation of an EDZ around tunnels in crystalline rocks is generally accepted and applied in the nuclear waste industry (Martin & Christiansson, 2009; Siren et al., 2015), a variety of different concepts and methodologies exist for the assessment of the long-term EDZ development. Since the seminal work of Bieniawski (1967), it is commonly assumed that the long-term strength is associated with a stress level that marks the transition between stable and unstable crack growth (crack damage threshold, CD). At this damage threshold, cracks that were initiated individually begin to interact with each other and lead to rapid failure under continued loading (Diederichs, 2007). This stress level is typically found at around 80-90% of the short-term strength. A vast amount of static fatigue tests at different environmental conditions and stress levels ranging from the short-term strength to stress levels below the crack damage threshold has been performed (mainly in the radioactive waste community; e.g. Peng, 1971; Schmidtke & Lajtai, 1985) and demonstrated that time-dependent failure may also occur at stress levels below the CD threshold. These test results (i.e. time to failure at various stress levels) have been extrapolated to long service times of tunnels and are often used to predict the long-term development of the excavation damage and disturbance zone around repository tunnels (Damjanac & Fairhurst, 2010; Paraskevopoulou et al., 2018).

Deep geological repositories are expected to remain functional for more than 100,000 years. Therefore, understanding the long-term strength of the host rock, in addition to its short-term strength, is crucial. The factors controlling its time-dependent behaviour must also be considered when assessing the integrity of the underground infrastructure from construction through the operational phase. Time-dependent and progressive failure (Terzaghi, 1962) involves gradual internal structural changes within a rock mass resulting from incremental, slow damage

accumulation and localized weakening (e.g., rock-bridge failure), which can eventually lead to large-scale failure. The mechanisms and rate of progressive rock failure are influenced by a combination of external forces (e.g., temperature fluctuations, water infiltration, seismic activity, loading and unloading, etc.) and internal properties (e.g., rock composition, structural discontinuities, matrix porosity, rock bridge characteristics, etc.). Processes of long-term crack development in crystalline rocks are often associated with stress corrosion and sub-critical crack growth in chemically reactive environments (Nara & Kaneko, 2006; Nara et al., 2010). This is specifically relevant for radioactive waste disposal with elevated rock temperatures and, for example, high calcium ion concentrations due to cementitious materials (Nara et al., 2010). The development of subcritical cracks stands as a primary contributor to time-dependent fracturing in rock, which impacts the long-term strength. The rate of crack growth depends on various parameters including the type of applied load (tensile or compressive), magnitude of stress relative to the short-term strength, as well as the environmental factors such as temperature, relative humidity and water chemistry.

Achieving a comprehensive understanding of brittle fracturing in crystalline rocks necessitates evaluating the spatial and temporal development of damage across various scales, from the micro-scale to the macro-scale (Figure 1). This paper presents the overview of the PRECODE mine-by experiment and associated laboratory experimental framework at BedrettoLab, a new underground research laboratory (URL) in Switzerland. The PRECODE project combines multidisciplinary in-situ monitoring with controlled excavation methods and laboratory rock mechanics testing to investigate the mechanisms governing EDZ formation and evolution in crystalline rock. The resulting multi-scale dataset provides a basis for improving the understanding and prediction of EDZ evolution and its implications for the long-term performance of deep geological repositories.

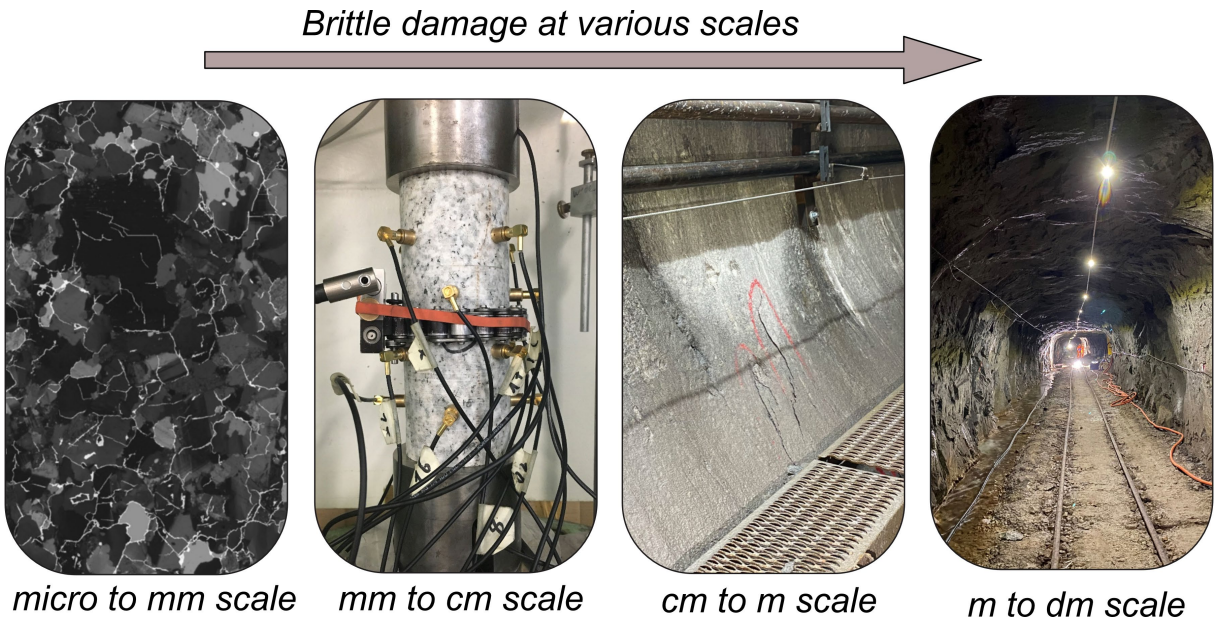


Figure 1: Illustration of the brittle damage in crystalline rocks at various scales

2. State-*of-the-art across Scales*

2.1 Laboratory Scale

Early studies have shown that brittle rock failure, particularly under low confining pressure, is controlled by extensional fractures rather than shear fractures (Cook, 1965; Hoek & Bieniawski, 1965; Bieniawski, 1967a, 1967b; Tapponnier & Brace, 1976; Horii & Nemat-Nasser, 1985; Martin,

1997). At the laboratory scale, the brittle failure of intact rock subjected to uniaxial or triaxial compression typically comprises four distinct stages: crack closure, elastic region, stable crack growth, and unstable crack growth (Martin & Chandler, 1994; Reches & Lockner, 1994; Eberhardt et al., 1999). Non-destructive monitoring methods, including axial and lateral strain measurements and acoustic emission (AE) monitoring, have been used to identify these stages and characterize the progressive damage evolution in brittle rocks (Martin, 1993; Eberhardt, 1998; Eberhardt et al., 1999; M. S. Diederichs et al., 2004; Cai et al., 2004).

The crack closure represents the first stage of the brittle fracturing process and is characterized by progressive closure of pre-existing microcracks, resulting in a nonlinear trend in the axial–lateral strain relationship before the onset of linear elastic deformation (Eberhardt, 1998). Following crack closure, the rock undergoes linear elastic deformation. The elastic properties such as Young's modulus and Poisson's ratio can be derived. Crack initiation is the start of micro-fracturing. During a compression test, this threshold can be identified when the lateral or volumetric strain responses depart from linearity or as the point at which a systematic increase in acoustic emission activity is first observed (Eberhardt, 1998). Cracks at this stage initiate in isolation and stop forming when loading stops or decreases (Eberhardt, 1998). Experimental results and in-situ observations have shown that crack initiation typically occurs when the applied stress level reaches approximately 30-50% of the peak uniaxial compressive strength (UCS) (Scholz, 1968; Lockner et al., 1991; Martin & Chandler, 1994; Martin, 1997; Eberhardt, 1998). With continued loading, crack growth remains stable until the start of unstable crack growth (CD threshold) (Reches & Lockner, 1994). In low porosity crystalline rocks under unconfined compression conditions, the CD threshold coincides at the point where volumetric strain reversal occurs (Amann et al., 2011). Using AE measurements, this threshold is determined by a marked increase in acoustic emission activity (Eberhardt, 1998). Unstable crack growth proceeds until microcracks coalesce into larger fractures, leading to peak strength and ultimate failure of the rock samples.

Recent advances in laboratory-scale rock mechanics have substantially improved the characterization of brittle fracturing processes in crystalline rocks under stress conditions relevant to deep geological repositories for nuclear waste. The integration of fiber-optic sensing techniques, including Distributed Strain Sensing (DSS), has enabled continuous, spatially resolved strain monitoring along the outer periphery of laboratory specimens, providing further insight into the initiation and propagation of brittle damage zones at the specimen scale (Hegger et al., 2022; Salazar et al., 2022; Salazar Vásquez et al., 2024; Bianchi et al., 2024; Chen et al., 2025). The monitoring of surface strain fields using digital image correlation (DIC) has also provided a more robust understanding of failure in brittle rock (e.g. Dutler et al., 2018; Torsello et al., 2026). Significant progress has also been made in understanding time-dependent brittle fracturing and long-term strength degradation through relaxation and static fatigue (Paraskevopoulou et al., 2016, 2018), subcritical crack growth and stress corrosion experiments (Nara, Takada, et al., 2010; Hamdi et al., 2026). Laboratory studies using double-torsion and fracture toughness testing under controlled temperature, relative humidity, and pore-fluid chemistry have shown that environmental conditions strongly affect crack growth rates and time-to-failure in crystalline rocks (Brantut et al., 2013; Nara et al., 2013). Adsorption-induced softening of rock caused by humidity and/or water saturation have been shown to significantly affect rock performance within environments expected in many underground excavation sites (Wu et al., 2023). Finally, advances in microstructural and multiscale analysis have strengthened the mechanistic understanding of brittle fracture processes and their upscaling to repository-scale behavior. High-resolution microscopy, micro-CT imaging, and micro-indentation testing have revealed the grain-scale controls on crack initiation, the influence of mineralogical

heterogeneity, and the role of pre-existing microstructures such as grain boundaries and healed fractures (Nasseri et al., 2005; Renard et al., 2019; M. Li et al., 2020; Winhausen et al., 2021)

2.2 Underground Research Laboratories

The definition of the EDZ to describe the extent and characteristics of the damage zones around tunnels has evolved over time (Tsang et al., 2005; Siren et al., 2015; Perras & Diederichs, 2016). In an attempt to standardize the EDZ definitions, Tsang et al. (2005) provided a comprehensive description of various damage zones around tunnels applicable for nuclear waste repositories. The characteristics of the damage surrounding tunnels depend on various parameters, such as tunnel shape, rock strength, initial stress conditions, excavation method, and the geometrical and mechanical properties of pre-existing discontinuities (Figure 2). The extent of the construction-induced damage (CDZ) can vary and depends on the excavation method used, i.e., drill & blast (D&B) or mechanical excavation, and can be minimized or potentially eliminated (Read, 2004; Martino et al., 2007; Jonsson et al., 2009). The highly damaged zone (HDZ), unlike the CDZ, is a direct result of stress redistribution due to the opening an excavation, and its extent is controlled by the geometry of the tunnel, structural features, the magnitude and orientation of stress. Visible stress-induced fractures develop in the HDZ, forming spalled blocks, outbreaks and interconnected macro cracks. Spalling to form a v-shaped notch is a typical example of the brittle damage within the HDZ (Read, 2004) due to the maximum tangential stress being concentrated at two opposing locations around the excavation. Beyond that, the inner EDZ (EDZi), characterized by connected damage, gradually transitions to the outer EDZ (EDZo), with partially connected to isolated damage (Bossart et al., 2002). The damage in this zone is often characterized by the development of microcracks and can be detected, for instance, through borehole/core p-wave velocity measurements (Falls & Young, 1998). Beyond the inner and outer EDZ, there will be an excavation influence zone (EIZ) that is characterized by elastic and reversible changes of strain (Siren et al., 2015).

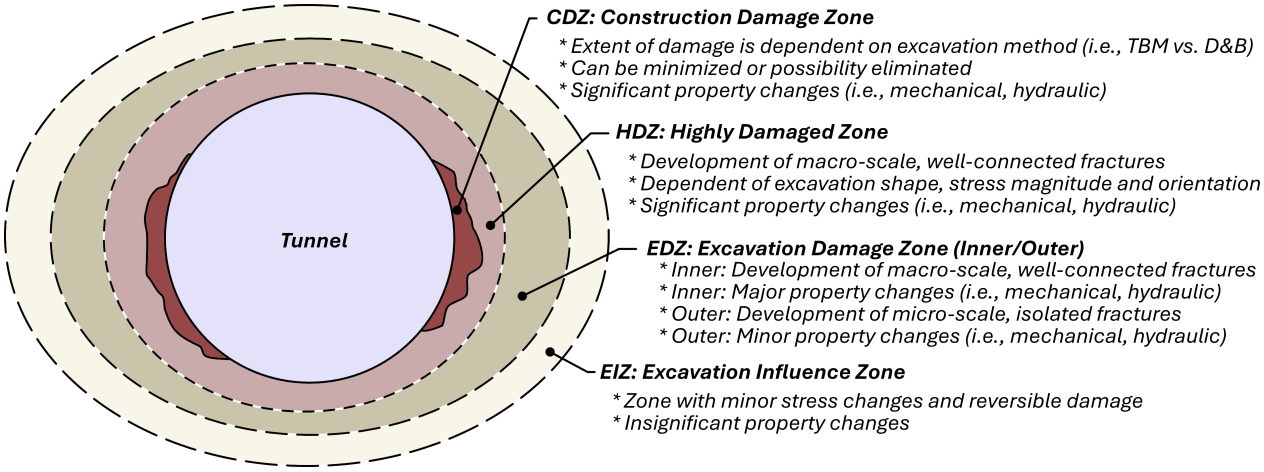


Figure 2: Definition of various damage zones around tunnels and their associated characteristics (modified after Siren et al., 2015; Perras & Diederichs, 2016)

In the context of nuclear waste disposal studies, several in-situ underground research laboratories (URLs) have been developed worldwide with the primary objective of investigating rock behavior at the repository scale, with an emphasis on the safety and feasibility of long-term storage. The focus on the surrounding rocks as a geological barrier is to understand the long-term thermo-hydro-mechanical (THM) behavior of the rock mass as a result of interaction with the nuclear waste. Some of the main URLs in crystalline rocks include: Äspö Hard Rock Laboratory (HRL) in Sweden, Onkalo Posiva Oy facility in Finland, AECL's Underground Research Laboratory

(URL), Grimsel Test Site in Switzerland, Mizunami URL (MIU) in Japan, Bukov Underground Research Facility in Czech Republic and Beishan underground URL in China. Many of these underground research laboratories have been constructed in a variety of rock types, at different depths, and using diverse excavation geometries and methods under varying environmental conditions, enabling systematic evaluation of their influence on EDZ characteristics. The following paragraphs summarize some of the key findings from these URLs.

The Mine-by Experiment in Canada at AECL's URL aimed to study the evolution of the progressive failure and development of the EDZ around a mechanically-excavated circular tunnel that was heavily instrumented prior to the excavation. Through analysis of several thousand microseismic and acoustic emission (MS/AE) events around Mine-by Experiment, Collins (1997) found that the majority of the events were concentrated in the roof and floor of the excavation where the differential stress was the highest. Brittle failures in the form of V-shape notches were developed, primarily in the roof and floor of the tunnel. The stress level at which the brittle fracturing was initiated around the tunnel was found to be 50-60% of the rock strength determined at the laboratory scale (Martin et al., 1997). The influence of the excavation shape and method on the extent of the EDZ was assessed within an Excavation Stability Study in the Canadian Mine-by Tunnel experiment. Using AE monitoring, Falls and Young (1998) compared the extent of the EDZ developed around two tunnels with similar geometry and stress levels but with different excavation methods, i.e. drill and blast (D&B) and tunnel boring machine (TBM). They found that the extent of the EDZ around the TBM tunnel was substantially less compared to the D&B tunnel, with the rate of AE counts being about ten times higher in the D&B tunnel compared to the TBM tunnel. Similar results were also obtained within ZEDEX project at Äspö HRL, Sweden and Onkalo site, Finland (Siren et al., 2015). Within the ZEDEX, the AE monitoring showed a distinct difference in observed EDZ extent caused by excavation methods i.e., D&B vs. TBM, with the depth of the EDZ for the D&B section estimated to be up to 1 meter from the tunnel wall, while for the TBM section the EDZ depth was limited to a few centimeters.

The hydraulic tests conducted prior and after excavation within ZEDEX project indicated that the preferential pathways for radionuclide transport were limited to the EDZ zone and no enhanced permeability was observed beyond that. The ZEDEX results indicated that the transition from the EDZ, which has irreversible changes, to the EIZ is gradual, with no distinct boundary that can be marked between the two zones through measurement methods (Bäckblom & Martin, 1999; Olsson et al., 2004). Results from a series of borehole hydraulic tests conducted as part of the EDZ experiment at the Grimsel Test Site indicated the presence of a zone approximately 1 m thick around the tunnel with permeability higher than that of the intact rock matrix, reflecting the development of an EDZ (Frieg et al., 2012).

Upon nuclear waste emplacement, heat transfer will occur from the canisters across bentonite buffer material towards the rock, with the canister surface temperature reaching up to 150 °C and a temperature of ~ 90 °C at the bentonite-rock interface (Bossart et al., 2017), depending on the specific design and layout of the repository. The Heated Failure Tests in the Canadian Mine-by tunnel studied the effect of thermally-induced stress on initiation of new cracks and propagation of the fractures. The Mine-by Heated Experiment showed the effect of thermally-induced stress on initiation of new cracks and propagation of the fractures that are in the critical-equilibrium state. Falls and Young (1998) reported a substantial increase in the number of AE counts around the region that was heated from ambient temperature to 85 °C. The in-situ monitoring of the AE development at the ASPE Experiment within the HRL in Sweden also indicated the development of thermally-induced fractures and growth of the EDZ caused by an increase in temperature (Andersson & Martin, 2009; Andersson et al., 2009).

2.3 Numerical Modelling of Spalling in Brittle Rocks

Over the past few decades, various numerical modeling approaches have been developed to simulate brittle failure and the characteristics of EDZ around underground openings. These include continuum methods (Martin et al., 1999; Hajiabdolmajid et al., 2002; Diederichs, 2007; Sanipour et al., 2022; Rógenes et al., 2024), discontinuum methods (Potyondy & Cundall, 2004; Shin et al., 2007; Rasmussen & Min, 2024; Potyondy & Fu, 2026), and hybrid methods (Lisjak et al., 2015; Hamdi et al., 2017; Vazaios et al., 2019; Potyondy et al., 2020).

Initial attempts to model the EDZ around Mine-by URL showed that the conventional constitutive laws with simultaneous mobilization of cohesion and friction angle failed to reproduce the depth and shape of the EDZ (Martin et al., 1999; Hajiabdolmajid et al., 2002). Using a Hoek-Brown constitutive model, Martin et al. (1999) showed the depth of failure around the URL test tunnel can only be simulated using elastic models when the Hoek-Brown parameters m and s are modified (m = 0, s = 0.11). Since that time, several other continuum methods have been proposed, with two common approaches being the Cohesion Weakening Frictional Strengthening (CWFS) (Hajiabdolmajid et al., 2002) and the Damage Initiation and Spalling Limit (DISL) (Diederichs, 2007). While, these methods can be able to simulate the depth and shape of failure around underground openings (Perras & Diederichs, 2016), they often fail to accurately predict the extent of the EDZ. This limitation arises from the continuum assumption, which prevents the explicit representation of fracture initiation and propagation, resulting in failure near excavation boundaries being predominantly represented as shear deformation. More recently, incorporation of the grain-like discontinuum concept (i.e., Voronoi Tessellated Model, VTM) into continuum models have shown promising potential to simulate brittle fracturing by incorporating heterogeneities with continuum methods (Sanipour, 2021; Rógenes et al., 2024).

Discontinuum methods (i.e., discrete element method, bonded-block models or bonded-particle models) simulate the rock domain as an assembly of blocks/particles that are joined together at their contact interfaces Potyondy & Cundall, 2004). These models explicitly account for material discontinuities and the heterogeneous grain-scale structure of rock and can simulate the progressive brittle failure though breakage of bondage. Since the seminal work of Potyondy & Cundall (2004) to model the observed failure around Mine-by URL in Canada using PFC software, numerous studies have investigated the capability of discontinuum methods to replicate brittle fracture processes. Using the Grain-Based Model (GBM) in UDEC, Shin et al. (2007) successfully reproduced both the depth and shape of spalling around the Mine-by tunnel and demonstrated the importance of grain geometry and heterogeneity in simulating spalling damage. More recently, Potyondy & Fu (2026), reviewed the historical development of discontinuum bonded-particle models and discussed their application to the simulation of spalling failure around underground excavations.

Hybrid methods, such as the Finite–Discrete Element Method (FDEM), combine the advantages of both continuum and discontinuum approaches by simulating the transition from a continuous to a discontinuous state through the explicit modelling of fracture initiation, propagation, and coalescence (Munjiza, 2004). In recent years, several modelling benchmarks have focused on simulating the EDZ around the Mine-by URL tunnel in Canada. Using an FDEM approach, Hamdi et al. (2017) investigated the impact of micro-heterogeneity on the in-situ strength reduction of the massive Lac du Bonnet granite and attempted to reproduce the shape and depth of spalling around the Canadian Mine-by Tunnel. Using Irazu software based on FDEM method, Vazaios et al. (2019) simulated the V-shaped notch formation around the URL test tunnel. According to their results, a reduced uniaxial compressive strength (to 120 MPa) is needed to properly capture the depth of EDZ observed around the tunnel. More recently, Potyondy et al. (2020) used coupled

PFC3D/FLAC3D with various grain shapes (spherical, Voronoi, and tetrahedral) to assess the capability of the combined continuum-discontinuum model to simulate the spalling process at the URL test tunnel. Their results demonstrated that representing the rock mass using tetrahedral grain blocks provided the best agreement with the in-situ spalling depth.

3. Open Science Questions

Despite many advances in understanding the brittle fracturing in terms of its temporal and spatial evolution and across multiple scales, there still remain a number of open, fundamental questions. One key open question concerns the estimation of the long-term strength of brittle rocks at laboratory and repository scale. It is commonly assumed that the long-term strength is associated with a stress level that marks the transition between stable and unstable crack growth (CD threshold). A vast amount of static fatigue tests demonstrated, that time-dependent failure may also occur at stress levels below the CD threshold (Peng & Johnson, 1972; Schmidtke & Lajtai, 1985; Paraskevopoulou et al., 2018; Wang et al., 2026). These test results (i.e. time to failure at various stress levels) have been extrapolated to long service times of tunnels and are often used to predict the long-term development of the excavation damage and disturbance zone around repository tunnels. The majority of previous attempts to assess long-term strength, such as time-to-failure analysis, have relied on laboratory tests that were subjected to stress levels above the CI threshold. A different concept is needed to address time-dependent fracture propagation processes at stress levels close to and below CI. As the confining stress increases, time-dependent fracture formation and propagation occur at stress levels above the CI threshold but significantly below the crack damage threshold. Thus, static fatigue tests with low differential loads, conducted at relevant confining stresses of 4-6 MPa (representative of a tunnel at 1000-1500 m depth), need to be performed to characterize time-dependent processes in this zone. Commonly, time-to-failure tests are conducted under unconfined conditions, and thus, the influence of confining stress is often not addressed. From a rock mechanical perspective, a systematic experimental analysis of this aspect is currently lacking.

It is well established that time-dependent subcritical crack growth and stress corrosion are primary mechanisms controlling the long-term strength of brittle crystalline rocks (Atkinson, 1984; Brantut et al., 2013; Nara, 2015). However, the observational window available for studying time-dependent crack growth, particularly at repository scale, is orders of magnitude shorter than the expected lifespan of deep geological repositories, which extends over hundreds of thousands of years. Most data collected from in-situ experiments at existing URLs span only approximately 5–20 years, limiting our ability to fully characterize the long-term evolution of the excavation damage zone (EDZ), particularly beyond the initial post-excavation phase (Read, 2004; Jonsson et al., 2009; Mellanen et al., 2010; Frieg et al., 2012). This gap is further intensified by the influence of environmental factors such as relative humidity, temperature, and pore-water chemistry, which are known to significantly affect subcritical crack growth rates and permeability evolution in crystalline rocks. Extending observational capabilities to capture EDZ characteristics over longer timescales under natural stress and environmental perturbations is therefore essential to improve our understanding of long-term rock mass behavior and to strengthen the safety assessment of deep geological nuclear waste repositories.

Understanding the impact of fault activation and earthquakes on the integrity of deep geological nuclear waste repositories is of critical importance for long-term safety assessment. Tectonic fault reactivation whether driven by natural stress evolution, glacial loading and unloading, or anthropogenic activities can lead to coseismic and aseismic slip, stress redistribution, and permeability enhancement in the surrounding rock mass, potentially compromising engineered and geological barriers. Earthquake-induced deformation may alter the hydraulic properties of

faults and adjacent damage zones, creating preferential pathways for radionuclide migration and affecting repository isolation over geological timescales (Sibson, 1990; Faulkner et al., 2010; Cappa & Rutqvist, 2011; Yang et al., 2021). Laboratory experiments, in-situ observations, and numerical modeling studies have shown that even small stress perturbations can trigger slip on critically stressed faults, emphasizing the sensitivity of fault systems in crystalline host rocks (Scholz, 1968; Ortlepp, 2000; Y. Li et al., 2025). Consequently, international repository programs increasingly emphasize the need to characterize fault mechanics, seismic hazard to evaluate repository robustness under both seismic and aseismic fault activity scenarios (i.e., SKB Report, 2011).

Even a massive rock mass suitable as deep geological repository inherently may contain pre-existing microfractures, healed joints, veins, and mineral fabric anisotropies that influence their mechanical response. Experimental, field and numerical studies have shown that stress-induced fracturing around underground openings strongly interact with pre-existing discontinuities, which may act as stress concentrators and crack initiators and mechanical contrast with the host rock (Kranz, 1983; M. Diederichs, 2003; Hamdi et al., 2015). Laboratory observations indicate that microcrack initiation and propagation often preferentially occur along grain boundaries, tips of microcracks, or healed fractures, leading to earlier onset of damage and altering failure paths compared to truly flaw-free material (Eberhardt et al., 1999). At the tunnel scale, the interaction between stress-induced fractures and natural fracture networks governs the characteristics of EDZ (i.e., geometry, depth, and connectivity), with important implications for permeability evolution and long-term repository integrity.

4. Bedretto Tunnel

4.1 Bedretto Tunnel Description

Located near the Gotthard Pass in the Swiss Central Alps, the Bedretto Tunnel is a NW-SE sidetrack tunnel that connects the Furka Base Tunnel to the Bedretto Valley. The tunnel was constructed 1970s and 1980s using conventional drill & blast method, with the main purpose of transporting excavated material during construction of the Furka Base Tunnel. This horseshoe-shaped tunnel is 5.2 km long with dimensions of 2.8x2.8 meters. The tunnel axis is oriented approximately N317° W, with the southern portal (Bedretto Valley, TM0) at an elevation of about 1479.5 meters above sea level (a.s.l.), and the northern portal (Furka Tunnel, TM5220) at an elevation of about 1505.2 meters a.s.l. The tunnel passes through mountainous terrain characterized by highly variable overburden depths. Starting from the Bedretto Valley, the overburden depth gradually increases, reaching a maximum depth of approximately 1.6 km under Pizzo Rotondo at around TM3140. It then decreases to a depth of approximately 1.1 km at TM4200, before increasing again to approximately 1.3 km at TM5200. Apart from some sporadic steel-set lining support at challenging sections, the Bedretto Tunnel has been mostly left unsupported since its first construction.

4.2 Geological and Structural Setting

The Bedretto Tunnel is situated within the Gotthard Massif in the Central Swiss Alps and crosses three main geological units: 1) Tremola series, 2) Prato series and 3) Rotondo granite (Figure 3). Starting from the South Portal (Tunnel Meter, TM0), the tunnel passes through metamorphic rocks of the Helvetic domain. Between TM0 to TM 434, the tunnel is within Temola series. Between TM434 to TM 1138, the tunnel is located within Prato series (Val Nalps Gneiss). Beyond this point, the tunnel is situated within the Rotondo Granite, extending to TM5220 (Keller & Schneider, 1982). The Tremola series comprises a sequence of metasedimentary rocks, predominantly featuring mica gneisses, mica schists, hornblende schists, and hornblende gneisses (Rast, 2020). The

Prato series is part of the Val Nalps Gneiss Complex and is characterized by banded hornblende schists and amphibolites in the northern and southern part and mica gneisses and schists with lenses of amphibolites in the central part (Hafner, 1958; Rast, 2020). The Rotondo granite that encompasses majority of the Bedretto Tunnel is characterized as an equigranular to porphyritic, medium to coarse grained granite with a mineral content of quartz (25 – 35%), alkali feldspar (20 – 40%), plagioclase (10 – 25%), biotite (3 – 8%) and garnet, phengite, chlorite, epidote, apatite and zircon as accessory minerals (Hafner, 1958; V. Lützenkirchen & Loew, 2011; Rast, 2020).

Geological structures including fracture sets and fault zones with various persistence and thickness ranging from sub-meters to tens of meters are frequently observed along the tunnel. Extensive surface and subsurface mapping of the geological structures has recently been conducted to analyze the geometrical and geomechanical characteristics of the structures in the study area (Lützenkirchen, 2002; Lützenkirchen & Loew, 2011; Jordan, 2019; Achtziger-Zupančič et al., 2024; Ceccato et al., 2024). Achtziger-Zupančič et al., (2024) identified three main sets of lineaments with different characteristics e.g., orientation, spatial distribution, persistence and intensity. They include: 1) NE-SW to ENE-WSW-striking lineaments with lateral persistence up to several hundreds of meters, 2) N-S striking structures with limited lateral persistency, and 3) WNW-ESE to NW-SE trending lineaments, with limited intensity and lateral persistency. Achtziger-Zupančič et al. (2024) further studied the chronology between the identified lineament sets, and identified a complex series of brittle, ductile and ductile-to-brittle shear zones that have imposed within the Rotondo granite. Further details on the geological and tectonic setting of the Bedretto Valley are provided in recent publications on BedrettoLab (Ceccato et al., 2024, 2026).

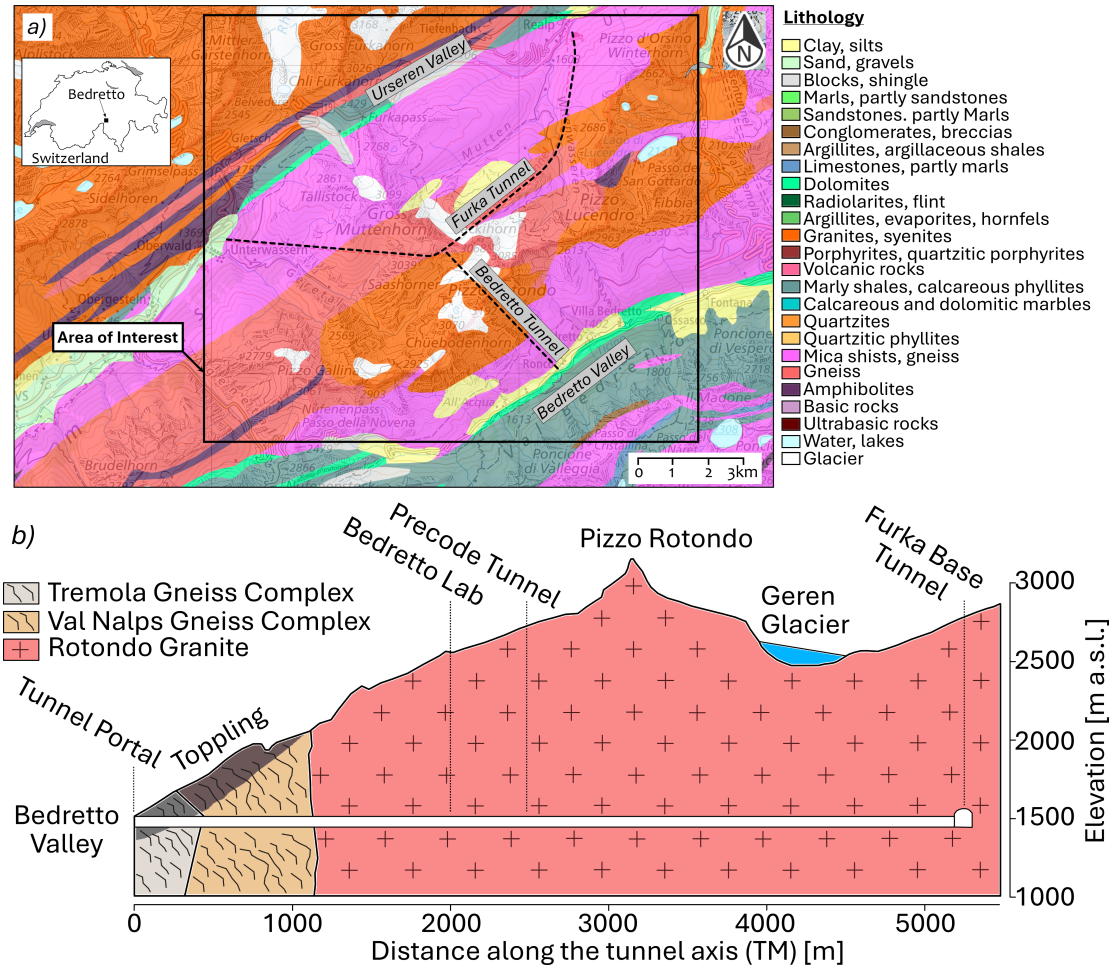


Figure 3: a) Lithology of the Bedretto Valley (source: SwissTopo), b) cross section along Bedretto Tunnel, with highlighted location of BedrettoLab and PRECODE Tunnel (modified after Keller & Schneider, 1982)

4.3 Hydro-Mechanical Laboratory Characterization

At a first approximation, the Rotondo granite within the Bedretto tunnel can be considered as homogeneous and isotropic medium, although a weak foliation due to ductile deformation during the Variscan orogeny is identifiable in various locations (Lützenkirchen & Loew, 2011). The petrophysical, mechanical and hydraulic properties of the Rotondo granite have been extensively studied under framework of the ongoing projects at the BedrettoLab (David et al., 2020; Ma et al., 2022; Perras et al., 2024; Hamdi et al., 2026; Kruszewski et al., 2026). A comprehensive laboratory testing program has been conducted as part of the PRECODE project, in order to identify the primary brittle fracturing thresholds needed to predict the extent of the EDZ in the Rotondo granite around the mine-by tunnel. These include uniaxial and triaxial compression tests, indirect and direct tensile, permeability, fracture toughness and petrophysical tests. Table 1 provides an overview of the average petrophysical and mechanical properties of the Rotondo Granite derived from samples collected in the Bedretto Tunnel.

Table 1: Average petrophysical and mechanical properties of the Rotondo Granite obtained from the Bedretto Tunnel (modified after Ma et al., 2022; Perras et al., 2024)

	Parameter	Units	Value
Mechanical Properties	Young's Modulus	GPa	52.5
	Poisson's Ratio	-	0.22
	Indirect Tensile Strength (BTS)	MPa	7.0
	Uniaxial Compressive Strength (UCS)	MPa	180.9
	Crack Initiation (CI)	MPa	64.5
	Crack Damage (CD)	MPa	117.0
Petrophysical Properties	P-wave Velocity	km/sec	3.4
	S-wave Velocity	km/sec	2.0
	Connected Porosity	(%)	1.36
	Dry Density	Kg/m^3	2606
Hydromechanical Properties	Permeability	m^2	$4.4e^{-18}$

4.4 Stress Measurement

The Bedretto valley has a complex tectonic history, with three distinct metamorphic phases (Labhart, 2005), Alpine uplift, erosion, glaciation/deglaciation, ductile and brittle deformation, resulting in a highly variable distribution of the field stress tensor. Due to the very low level of seismic activity in the Ticino region, including the Bedretto area, the use of focal mechanism solutions to infer the in-situ stress field is limited (Sue et al., 2007). In recent years, a series of in-situ stress measurement campaigns, mainly based on the mini-frac method, have been conducted at BedrettoLab to quantify the magnitude and orientation of the in-situ stress field along the tunnel (for more detail see: Ma et al., 2019; Bröker & Ma, 2022; Bröker et al., 2024). Overall, the stress state in the vicinity of the Bedretto Lab (TM2000) is found to be transitional between normal and strike-slip faulting (Shmin < SHmax ≤ Sv), with the estimated average stress magnitudes to be Shmin = 14.6 ± 1.4 MPa, SHmax = 25.4 ± 2.3 MPa and Sv ≈ 26.5 MPa (Bröker & Ma, 2022) between TM1750 and TM2250 with approximate overburden depth of 1030 m.

4.5 Excavation Damage Zone of the Existing Bedretto Tunnel

Frequent occurrences of buckling in the gneiss and spalling in the granitic zones were documented during the construction of the Furka and Bedretto tunnels (Amberg, 1983). Since its completion in 1982, the tunnel has remained largely unlined, providing a unique opportunity to investigate the long-term evolution of spalling and the excavation damage zone in crystalline rock. Several spalling characterization campaigns using conventional and remote sensing methods revealed that the depth and orientation of the excavation damage zone (EDZ) vary along

the tunnel in response to changes in topography and structures. The depth of spalling along the tunnel varies with the overburden, reaching values of up to 1.1–1.5 m in the most affected sections (Alcaino-Olivares et al., 2024; Hamdi et al., 2024, 2025). Huber (2004) divided the failure observed at the Bedretto Tunnel into three main categories of: 1) spall shears, 2) kink bands and 3) tension cracks. The spall shears are defined as the "onion-skin" surface parallel fractures that are formed in the area of maximum stress concentration with their thickness varying from a few millimeters to centimeters. The kink bands are triangular shaped fractures that are generally formed at the bottom and top of the spalled notches. The tension cracks are formed due to volumetric dilation in the slabs subjected to bending.

Continuous laser scanning of the tunnel wall conducted in 2024 between TM2400 and TM5200 (where the overburden ranges from 1.2 to 1.6 km) revealed that the excavation damage zone (EDZ) is asymmetrical, with its shape, position, and depth varying significantly along the tunnel. Systematic brittle fracturing and spalling have been observed along the tunnel particularly in the areas with higher magnitude of overburden between TM2000-5200. In addition, a number of sections along the tunnel show extensive overbreaks as a result of interaction between stress-induced fractures and pre-existing geological structures. The asymmetric shape of the EDZ indicates that the principal stresses are deviated from horizontal and vertical planes and are also not parallel to the tunnel axis, agreeing with current modelling results, in-situ stress measurements, and the regional stress field (Huber, 2004; Bröker & Ma, 2022; Alcaino-Olivares et al., 2024; Hamdi et al., 2025).

4.6 Environmental Condition at Bedretto

Keller & Schneider (1982) measured the temperature variation along the Bedretto Tunnel after completion of the tunnel construction. The rock temperature in the vicinity of the Bedretto Valley Portal (TM200) was 8°C, increasing to 18°C at TM2300 and remaining relatively unchanged until TM4200. The relative humidity at the Bedretto tunnel varies along the tunnel and may fluctuate seasonally, but the measurements have shown a high relative humidity, exceeding 80%. It is important to note that between 1984 and 2017, there was no door between the Furka Base Tunnel and the Bedretto Tunnel. As a result, the repeated passing of high-speed trains through the Furka Tunnel caused instantaneous cyclic changes in relative humidity between 80-100%, providing a more corrosive environment and allowing for a higher potential for subcritical crack growth during that time frame.

5. Development of a Novel Experimental Framework

5.1 PRECODE Project: Opportunities, Goals, and Objectives

The Bedretto Underground Laboratory (BedrettoLab) was established by ETH Zürich in 2018. During the initial phase, the in-situ experiments were conducted within the tunnel segment between TM2000 and TM2100, where the tunnel was widened to approximately 6 meters. The overburden in this segment ranges from roughly 1000 to 1030 meters. In the most recent phase, a new tunnel was excavated at TM2428, parallel to a fault zone on the southeast side of the existing Bedretto tunnel, with a length of approximately 100 m. This site currently hosts a number of large-scale in-situ experiments, with two of the relevant experiments being: (1) Fault Activation and Earthquake Rupture (FEAR), in which an isolated fault zone will be stimulated to seismogenic failure (Meier et al., 2026), and (2) Progressive Excavation Damage Zone Evolution During and Post Mine-By Tunneling (PRECODE), aimed at studying the development of the EDZ around crystalline rocks relevant for deep geological nuclear waste repositories. The primary objectives of the PRECODE project are to:

- Improve our understanding of the short-term rock mass behaviour due to tunnel advance with advanced monitoring systems that were not available for past granitic rock mine-by experiments (fiber optic strain sensing, distributed acoustic/strain sensing, micro-seismic sensors, LiDAR scanning, etc.),
- Improve our understanding of the influence of natural repository perturbations (humidity, temperature, seismicity, etc.) on progressive microcrack development within the EDZ over the long-term,
- Determine changes in EDZ's permeability with time under open (worst case) adit conditions
- Analyze the impact of tunneling on dislocations across fault zones and related changes in hydraulic properties
- Quantify the impact of activation of nearby faults on the EDZ characteristics and potential permeability enhancement

The research addresses brittle fracturing across multiple spatial scales (micro-, laboratory-, and in-situ scales) and temporal scales (short-, medium-, and long-term), using a range of complementary approaches organized into three major work packages:

(1) **Multi-disciplinary in-situ monitoring:** with a focus on detecting and quantifying the spatial and temporal development of the EDZ around the tunnel using various approaches, including passive and active seismic monitoring, hydraulic monitoring, geophysical monitoring, and deformation monitoring,

(2) **Comprehensive laboratory testing:** with a focus on deriving the short-term and long-term strength of the Rotondo Granite under various stress states (e.g., uniaxial and triaxial compression, indirect and direct tension, fatigue, relaxation) and environmental conditions (temperature, relative humidity, and water chemistry),

(3) **Advanced numerical modelling:** Using the seismo-hydro-mechanical dataset obtained from in-situ monitoring and laboratory experiments, to evaluate the capability of modelling approaches to predict the geometry and depth of failure, as well as the extent of the EDZ around the test tunnel.

5.2 Construction of PRECODE Mine-by Tunnel

Within the PRECODE Project, a new 100 m long side tunnel was excavated between 2024-2025 as a branch from the existing Bedretto tunnel (Figure 4). The azimuth of the new tunnel is S245°W and is 72° angled from the Bedretto Tunnel, which has an azimuth of N317°W. Before and during the mine-by excavation, the vicinity of the tunnel was densely instrumented with various sensors to monitor the evolution of the EDZ over a period of a few years. The tunnel was excavated at TM 2428 with approximate overburden depth of 1300 m, sufficient to create stress-induced brittle fracturing in the form of spalling. To assess the impact of construction-induced damage (CDZ) on the development of the EDZ, two excavation methods were employed during the construction of the PRECODE Tunnel: 1) controlled drill and blast (D&B), and 2) line drilling and rock breaking (LDRB), internally known as "soft excavation". The comparison between the LDRB and D&B sections allowed quantification of the EDZ resulting from stress redistribution alone and the EDZ resulting from both the construction method and stress redistribution. The first 10 m of the tunnel was built using D&B. The D&B excavation was carried out in 2024, with an average advance rate of 1 m/day. The subsequent 11 m were excavated using LDRB to minimize the influence of the excavation method on the development of the EDZ. The LDRB procedure involved drilling a series of perimeter boreholes along the intended tunnel profile to decouple the outer perimeter from the inner rock mass. The inner section was then sequentially removed using a rock splitter and a rock hammer. After 4 m of advance using LDRB, excavation was paused to allow for the drilling and

instrumentation of a series of radial boreholes equipped with hydraulic and deformation monitoring sensors; after that the LDRB was continued for another 7 m (more details in Section 5.3). The construction of the LDRB section was significantly slower than the D&B section, with an average advance rate of 0.1-0.25 m/day. The excavation of the PRECODE section (the first 21 m) was completed in October 2024 (Figure 5). The excavation was then continued for an additional ~80 m using D&B method to create an Earthquake Physics Testbed (ETB) for the FEAR experiment (Meier et al., 2026).

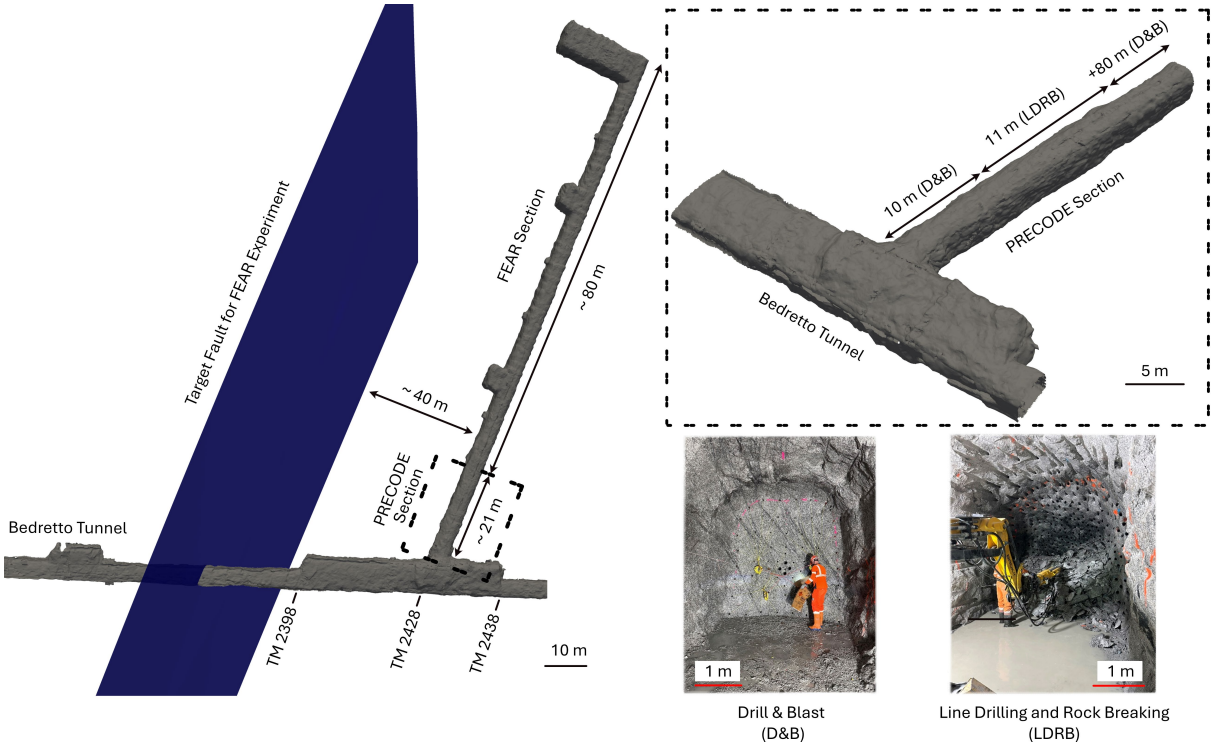


Figure 4: Left: Isometric view of the Bedretto Tunnel and the newly-excavated PRECODE/FEAR Tunnel, Right: As-built geometry of the PRECODE Section, showing D&B and LDRB sections

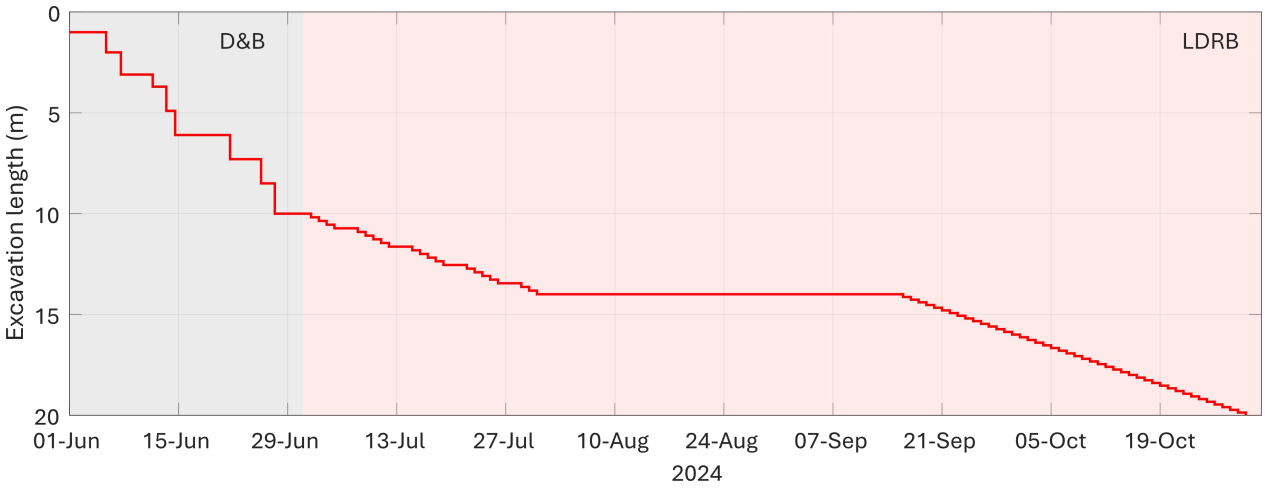


Figure 5: Excavation advancement for the PRECODE section

5.3 Multi-Disciplinary In-situ Monitoring

Comprehensive multidisciplinary surface and borehole monitoring was implemented before and during the construction of the PRECODE section to investigate the spatial and temporal evolution of the EDZ, the impact of tunneling, post-construction permeability enhancement, the influence

of excavation methods on EDZ characteristics, and impact of fault-activation on EDZ. A series of longitudinal and radial boreholes were drilled and instrumented prior to the start of tunnel excavation, enabling monitoring of the development of the EDZ and its impact on the surrounding rock mass during excavation and in the post-excavation phase (Shakas et al., 2026). In addition to borehole monitoring, a series of surface-based measurements including terrestrial laser scanning (TLS), surface ground-penetrating radar (GPR), electrical resistivity tomography (ERT) and fracture mapping were carried out, complementing the borehole observations. Table 3 and Figure 6 present details of the boreholes drilled prior to and during tunnel construction, along with the corresponding installed sensors.

Table 2: Overview of drilled boreholes and their respective configurations around PRECODE Mine-by Tunnel

Borehole Name	Borehole Type	Length (m)	Dip from Hz. (- deg down)	direction (deg)	Diameter (mm)	Purpose
BPR_01	Longitudinal	25	2	245	96	Passive and active seismic monitoring
BPR_02		25	2	245	96	
BPR_03		25	2	245	96	
BPR_04		25	2	245	96	
BPR_05		22	-6	233	96	
BPR_06		3	80	245	96	
BPR_07		3	80	245	96	
BPR_08	Longitudinal	8.5	-5	231	76	Hydraulic monitoring
BPR_09	Longitudinal	23	-4	245	76	Characterization hole
BPR_10	Radial	5	-2	335	76	Hydraulic monitoring
BPR_11		5	-2	335	76	
BPR_12	Radial	5	-5	335	96	Deformation monitoring
BPR_13	Radial	2	-10	335	45	Geophysical monitoring
BPR_14		2	-10	335	45	
BPR_15		2	-10	335	45	
BPR_16		2	-10	335	45	

Active and Passive Seismic Monitoring: The seismic monitoring network was installed prior to initial drill-and-blast excavation phase and was designed to track the transient evolution of microcracking in the damage zone during and after excavation. The network was designed with increased sensitivity during the four- and seven-meter soft excavation phases, while sensitivity was lower during the initial drill-and-blast phase. Additionally, as excavation progressed, sensors were excluded from the location procedure once the direct rays from the microcracks to the sensors passed through the newly excavated void space. The network comprised a total of 31 in situ acoustic emission (AE) sensors, placed in five longitudinal boreholes approximately one meter from the tunnel wall (Figure 6, yellow cones). Four of these boreholes (BPR_01 to BPR_04) were dry, drilled with a 2° upward dip, and housed 27 AE sensors (GMuG-BLw-7-70) equipped with curved front surfaces. These sensors were deployed in shuttles, where spring cylinders ensured contact with the borehole walls. The fifth borehole (BPR_05), drilled with a 6° downward dip beneath the tunnel, contained four AE sensors (GMuG-BLc-30-60). In addition to the AE sensors, the borehole was equipped with distributed acoustic sensing (DAS) and distributed strain sensing (DSS) cables and was subsequently grouted. The AE sensors, manufactured by

Gesellschaft für Materialprüfung und Geophysik GmbH (GMuG), operate within a bandwidth of 1 to 100 kHz, with peak sensitivity at 70 kHz. For calibration, two steeply upward-dipping boreholes (BPR_06 and BPR_07) at the tunnel entrance were instrumented with one AE sensor (GMuG-BLw-7-70), two one-component (1C) accelerometer (Wilcoxon 736T), and a three-component (3C) accelerometers (Endevco 45A). The accelerometers are indicated by red cones in Figure 6. Additionally, three seismic sources were distributed across three different boreholes for active seismic surveys (Figure 6, pink cones). The data acquisition systems of the network acquired continuous data at a sampling rate of 200kHz. The continuous data was processed using the SeisComp seismological software package (Helmholtz-Centre Potsdam-GFZ German Research Centre For Geosciences & GEMPA GmbH, 2008). Due to elevated noise levels during excavation and other tunnel operations, AE data was analyzed exclusively during periods when no personnel were present in the tunnel.

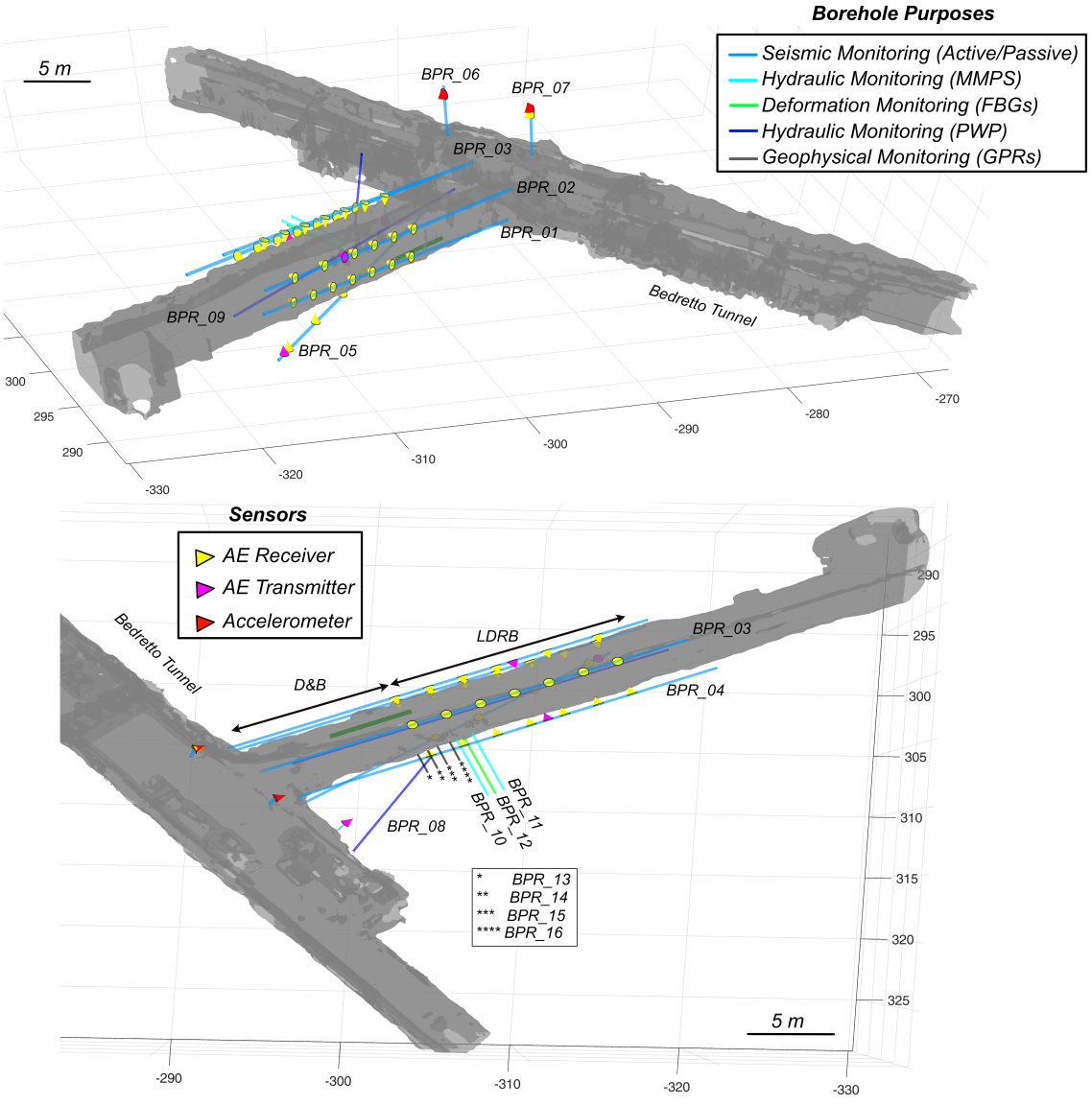


Figure 6: Multidisciplinary monitoring scheme of the PRECODE Section

Pore Pressure Monitoring: The BPR_08 borehole, with a diameter of 76 mm and a total length of 8.4 m, was drilled diagonally toward the PRECODE tunnel along an azimuth of S231°W with a downward inclination of approximately 5°. This borehole trajectory was chosen to enable pore pressure and permeability measurements at three monitoring intervals located at distances of

4.3 m, 2.3 m, and 1.1 m from the tunnel wall. Following coring, comprehensive borehole geophysical logging was performed, including ground-penetrating radar (GPR), acoustic televiewer (ATV), and optical televiewer (OTV) surveys. These logs were used to select monitoring sections within intact, unfractured parts of the borehole, ensuring that the measurements represent intact rock properties rather than fracture-dominated flow. The borehole was then equipped with a multi-packer system to hydraulically isolate the monitoring intervals using inflatable rubber packers. To further improve sealing, particularly in the presence of pre-existing or excavation-induced open fractures and to prevent cross-flow between adjacent sections, three additional borehole segments with lengths of 1.0 m, 0.5 m, and 0.5 m were filled with resin. Pore pressure is monitored in real-time in three isolated intervals with lengths of 0.14 m, 0.23 m, and 0.23 m, respectively. Pressure measurements started immediately after installation of the monitoring system on 21 March 2024 using Keller pressure sensors operating at a sampling frequency of 5.56×10^{-4} Hz, with an accuracy of ±0.1 kPa, a resolution of 0.01 kPa, and a pressure rating of 10 MPa. Hydraulic pulse injection tests using clean water with overpressures of approximately 0.3 MPa, as well as pulse withdrawal tests, were conducted in the isolated monitoring intervals before, during and after PRECODE tunnel excavation.

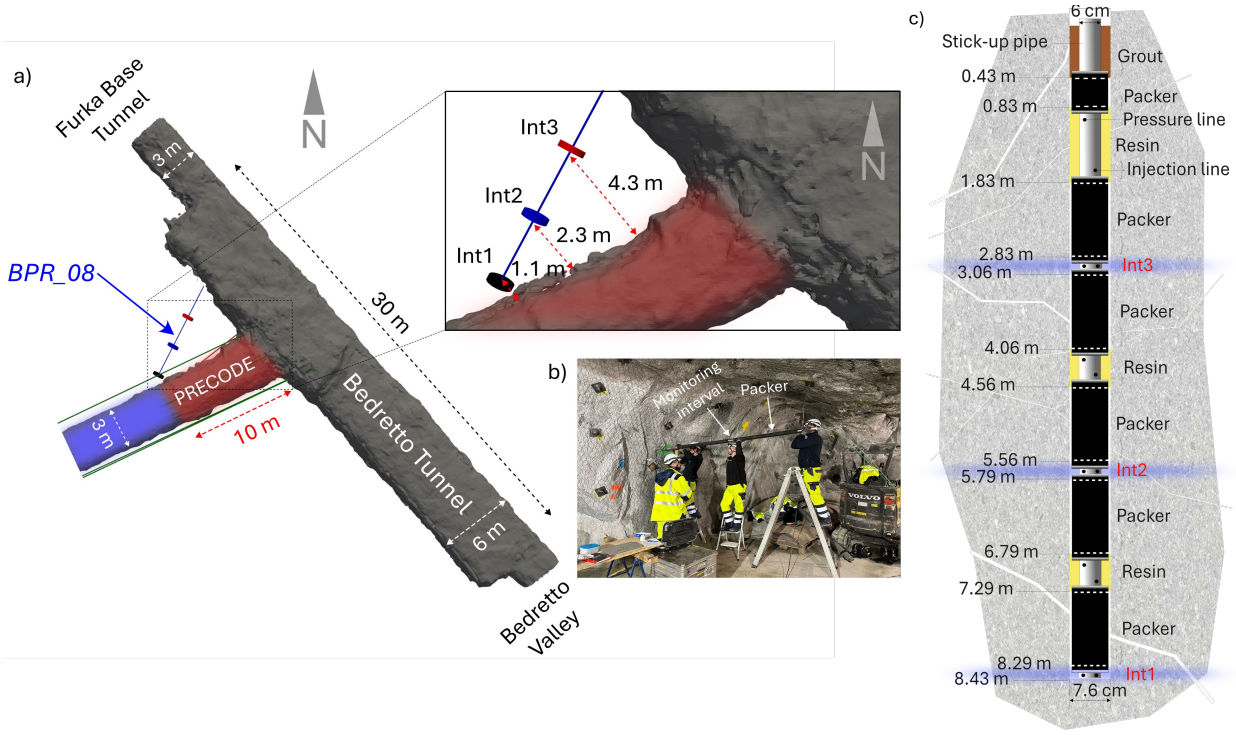


Figure 7: a) Instrumentation of the BPR_08 pressure monitoring borehole during the PRECODE experiment; b) an image of the packer system during installation, c) the detail of the three monitoring intervals

Active Hydraulic Monitoring: Active hydraulic testing was conducted in two radial, sub-parallel boreholes (BPR_B_10 at TM 10.75 and BPR_B_11 at TM 11.75; Table 3 & Figure 6), drilled immediately after excavation of the first 4 m of the LDRB part of the PRECODE tunnel (TM 14). The boreholes were drilled sub-horizontally (~2° downward) into the NW wall of the mechanically excavated tunnel section at a height of approximately 1.20 m above the tunnel floor. In August 2024, two modular multi-packer systems (MMPS; manufactured by Solexperts AG) were installed in each of the ~5 m long boreholes. In each borehole, four test intervals were hydraulically isolated by four inflated rubber packers with sleeve lengths of 0.25 m and 0.50 m (Figure 8), with identical configurations between both boreholes. Interval spacing decreases toward the tunnel wall to achieve high spatial resolution, enabling detailed characterization of the EDZ. The deepest

interval (Int1) extends from the deepest packer (Pa1) to the borehole end (Figure 8). The interval positions and lengths are summarized in Table 4.

The MMPS installations were designed to remain in place during continued tunnel excavation and after completion, allowing continuous pore-pressure monitoring and repeated hydraulic testing at fixed interval positions to characterize the spatial and temporal evolution of the EDZ. A series of hydraulic and pneumatic in-situ tests was performed and repeated over several field campaigns to evaluate interval permeabilities. These tests include pulse injection and withdrawal tests, constant head tests, and constant rate tests. Gas tests were limited to the unsaturated intervals, closest to the tunnel wall (Int4), where atmospheric or sub-atmospheric pressures were measured, indicating suction effects ($P_{int} \leq P_{atm}$).

Table 3: Borehole interval positions in BPR_B_10 and -11

Interval Name	Start depth [m]	End depth [m]	Interval length [m]
Int1	2.28	5.06	2.78
Int2	1.58	1.78	0.20
Int3	0.88	1.08	0.20
Int4	0.43	0.63	0.20

Hydraulic testing was performed using an electric pressure pump (*REMS E-Push 2*) and a flowboard equipped with three *Bronkhorst Cori-Flow* flowmeters covering a flow-rate range from 0.017 to 667 ml/min. At a control board attached to the tunnel side wall, the packers and borehole intervals are connected via steel lines and monitored using manometers and digital pressure sensors (*Keller, type PAA-33X*). The system is designed to measure interval pressures of up to 10 MPa at a sampling frequency of 1 Hz. Interval pressures were continuously monitored and made remotely accessible. Pneumatic tests were conducted using N_2 for injection from a gas bottle and a dedicated gas flowboard equipped with three *Vögtlin* thermal mass flow meters (*red-y-smart series*) covering a flow-rate range from 0.25 ml_n/min to 100 l_n/min.

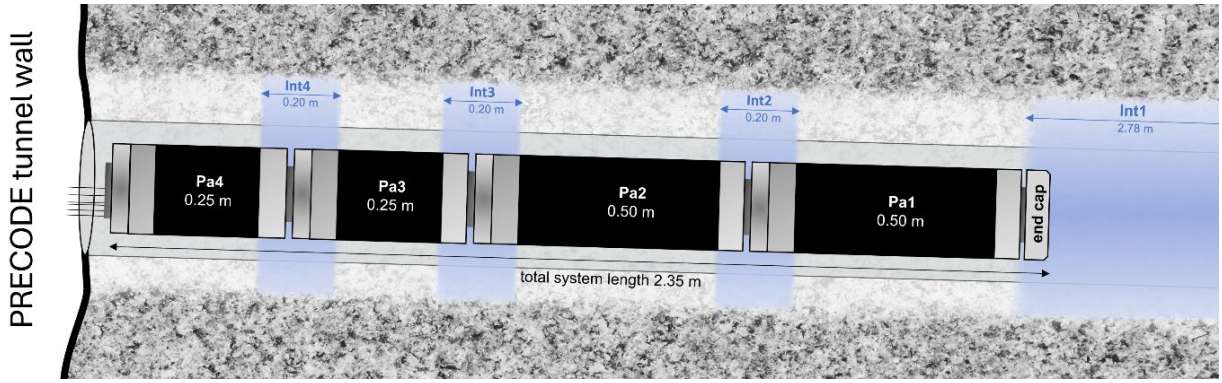


Figure 8: Schematic illustration of the modular multi-packer system (MMPS) installed in boreholes BPR_B_10 and BPR_B_11. The configuration is identical for both boreholes. Packer sleeve lengths (Pa1-Pa4) and the resulting hydraulically isolated test intervals are indicated (Int1-Int4)

Geophysical Monitoring: Geophysical monitoring consists of repeated borehole and tunnel measurements. The objective of the geophysical monitoring is to collect time lapse of EDZ evolution and allow for comparison of the shape and extent of the EDZ between areas with different excavation methods. In both the radial and longitudinal boreholes, we collected repeated optical/acoustic televiewer (OPTV/ATV from Advanced Logic Technologies) data to

characterize the EDZ around and ahead of tunnel face. The televiewer probes were run with a spacing of 5 mm and measurement was carried out after each round of excavation. In addition, we used borehole GPR with antennas from *GeoScanners AB* having central frequencies of 500 MHz and 1 GHz. The profiles were collected with a trace spacing of 8 mm using a triggering wheel and cable markers for precise location. For time-lapse imaging, we installed two electrical resistivity arrays along the tunnel wall as shown in Figure 9a. We designed the profile geometry to traverse from the drill and blast to the soft excavation part of the experiment, with the transition roughly at the middle of the profile. Each profile consists of 50 electrodes, separated by 100 mm (Figure 9b) and therefore spans roughly 5 m. The profiles are horizontal and separated by a vertical distance of 0.5 m. To install the electrodes, we drilled into the rock at ~ 20 mm depth using 8 mm drill bits. We then cleaned the hole, filled it with graphite paste and pushed permanent, stainless steel bolts inside (Figure 9b). We tested various contact methods and the graphite paste was ideal to minimize the contact impedance between the metal and rock, while also reducing the risk of corrosion over time. The mechanical coupling of the bolts was firm due to their expandable nature, but some loose parts of the rock resulted in a total of 8 failed electrodes along the two profiles. The setup is permanent, and each electrode is connected to takeout from a custom-made multi-core cables attached to a *GeoTOM* electrical resistivity meter. We setup the acquisition so that Wenner, Schlumberger and Dipole-Dipole arrays are repeated every 3-days.

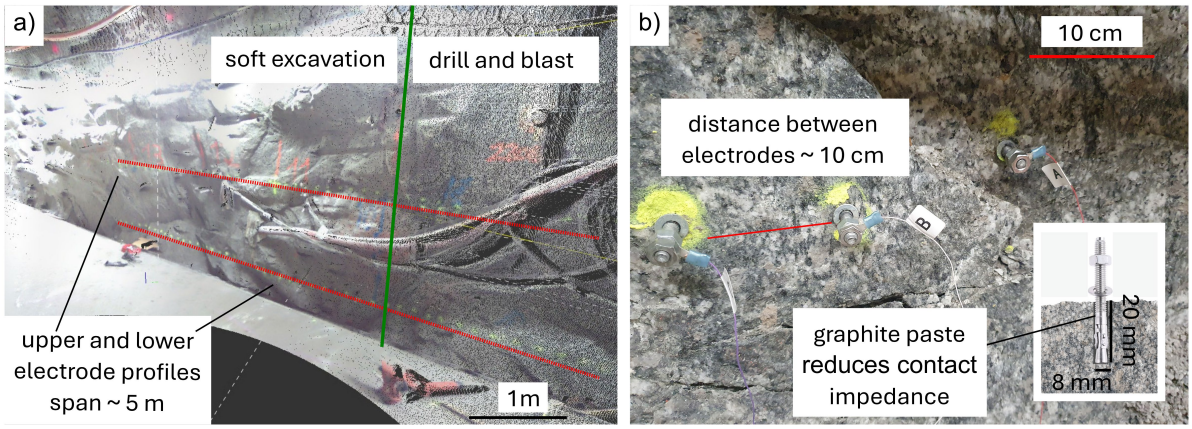
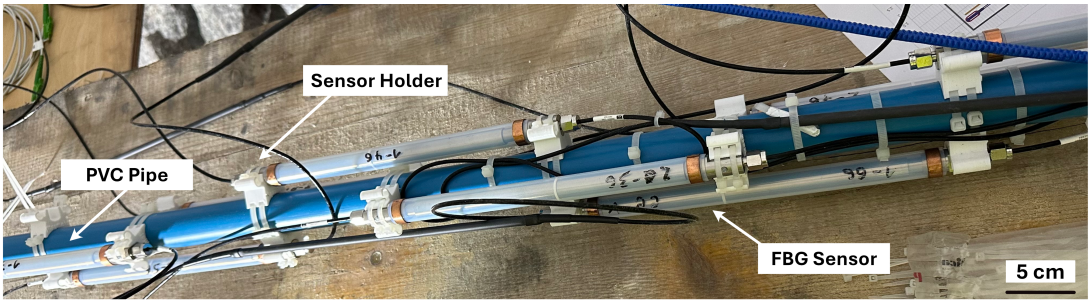


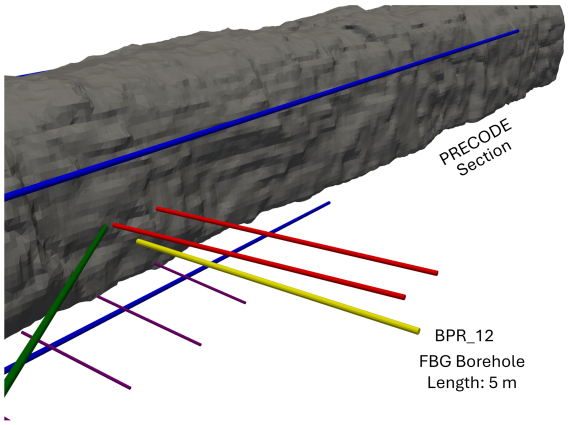
Figure 9: a) Illustration of the electrical resistivity profiles installed on the tunnel wall, that transverse between soft excavation and drill-and-blast. The image is derived from a laser scan (ref) and shows the roughness of the tunnel wall. b) A closeup picture of three electrodes, indicating the relevant dimensions and wall roughness

Deformation Monitoring: A radial borehole (BPR_12) was drilled in the tunnel sidewall approximately 1 m above the tunnel floor in an area prone to spalling concentration. The borehole was instrumented with a dense array of Fiber Bragg Grating (FBG) sensors and Distributed Strain Sensing (DSS) to monitor the evolution of deformation during and after excavation. The borehole was 5 m long, inclined downward at 5°, and had a diameter of 96 mm. In total, 16 FBG sensors (model: os3600 manufactured by Luna) were installed, of which 10 had a baselength of 25 cm and the remaining 6 had a baselength of 100 cm. The os3600 sensor has ± 2,500 με strain limits with strain sensitivity of ~ 1.2 pm/με with operating temperature range of -40 to 80 °C. The cables were pre-strained to allow for monitoring both extensional (opening) and contractional (closing) deformation. For the FBG sensors, emphasis was placed on high redundancy, ensuring that multiple sensors covered each cross-section at nearly every depth, with higher redundancy near the tunnel sidewall, where the EDZ concentration was greatest. The FBG sensors were arranged sequentially with overlapping coverage on a PVC pipe, with the first sensor located 6.5 cm inside the borehole mouth, allowing deformation to be captured immediately at the tunnel sidewall. To

provide additional redundancy and to accommodate wavelength limitations, the FBG sensors were divided into three separate chains, each with fiber access from both ends. A robust V13 cable was installed in a loop configuration to provide redundancy, with the loop formed using a Mini-Loop at the bottom of the borehole. The detailed depth of all sensors and other objects and additional information regarding the FBG sensors can be found in Figure 10. Upon placement of the senor's chain in the borehole, cementation was carried out using a hand-driven mixing and pumping system. In order to optimally fill the cavity of the borehole and guarantee a good bonding to the rock, a grout mixture containing bentonite, cement and water was mixed and injected from the bottom of the borehole to the borehole mount.



FBG ID	Chain	Bottom depth (cm)	Top depth (cm)	Baselength (cm)
FBG 1	Chain 2	431.5	331.5	100
FBG 2	Chain 1	366.5	266.5	100
FBG 3	Chain 3	356.5	256.5	100
FBG 4	Chain 2	331.5	231.5	100
FBG 5	Chain 1	266.5	166.5	100
FBG 6	Chain 3	231.5	131.5	100
FBG 7	Chain 2	144	119	25
FBG 8	Chain 1	131.5	106.5	25
FBG 9	Chain 2	119	94	25
FBG 10	Chain 1	106.5	81.5	25
FBG 11	Chain 3	94	69	25
FBG 12	Chain 3	81.5	56.5	25
FBG 13	Chain 2	69	44	25
FBG 14	Chain 1	56.5	31.5	25
FBG 15	Chain 2	44	19	25
FBG 16	Chain 1	31.5	6.5	25



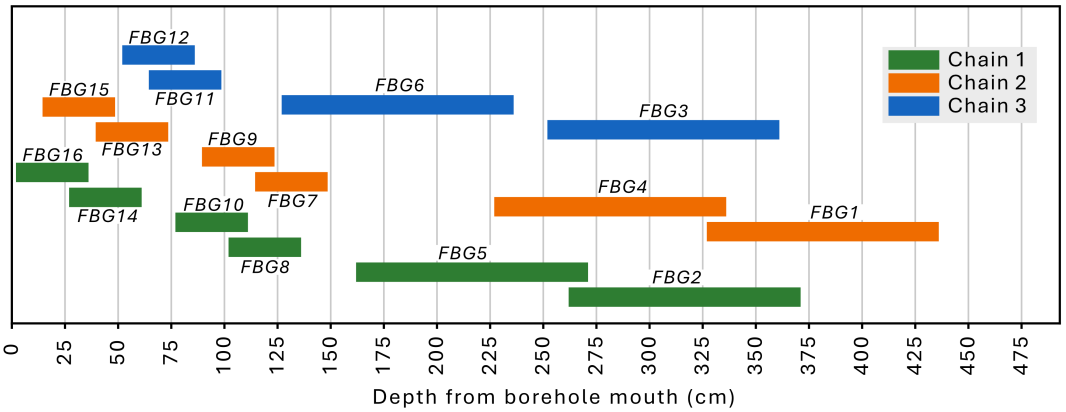


Figure 10: FBGs layout in BPR_12 borehole to monitor the development of deformation, Top: An example of the FBG array, Middle: list of installed FBGs and isometric view of the borehole, Bottom: schematic illustration of the installed FBG within the borehole and their overlaps

6. Preliminary Results and Interpretations

6.1 Brittle Damage Characterization through Acoustic Emission Monitoring

Acoustic emission (AE) monitoring started in June 2024, during the final phase of drill-and-blast (D&B) excavation, and continued until the end of the line drilling and rock breaking phase in early

November 2024. To minimize false positives, AE data processing was suspended during active excavation and other tunnel operations. The results of the AE monitoring as a function of time and excavation progress are shown in Figure 11. Figure 11a and Figure 11b indicate that significantly more AE events were recorded during the D&B phase than during excavation using the LDRB method. During the D&B phase, peaks in AE activity closely correspond to individual blasting rounds. During July 2024, when excavation was performed with the LDRB method, work was limited to weekdays, with no excavation on weekends. Following a break between August and early September, excavation resumed in mid-September and continued through weekends, which coincides with an increase in AE activity. Figure 11c shows the log-density distribution of AE events recorded during both excavation phases. A clear concentration of events occurs along the tunnel sidewalls, where stress concentrations are expected to be highest. The spatial distribution of AE events around the tunnel cross-section suggests that the maximum principal stress (σ_1), likely corresponding to the vertical stress in the PRECODE tunnel, may be inclined by approximately 15° relative to the vertical. The highest density of AE events occurs within approximately 1.5 m of the tunnel wall, which likely represents the maximum extent of the outer excavation damage zone (EDZ), including irreversibly micro-damaged rock with and without significant dilation. The highest concentration of AE events is observed within the first 0.5-0.6 m from the tunnel wall, which broadly corresponds to the zone of visible surface damage, including the CDZ and HDZ.

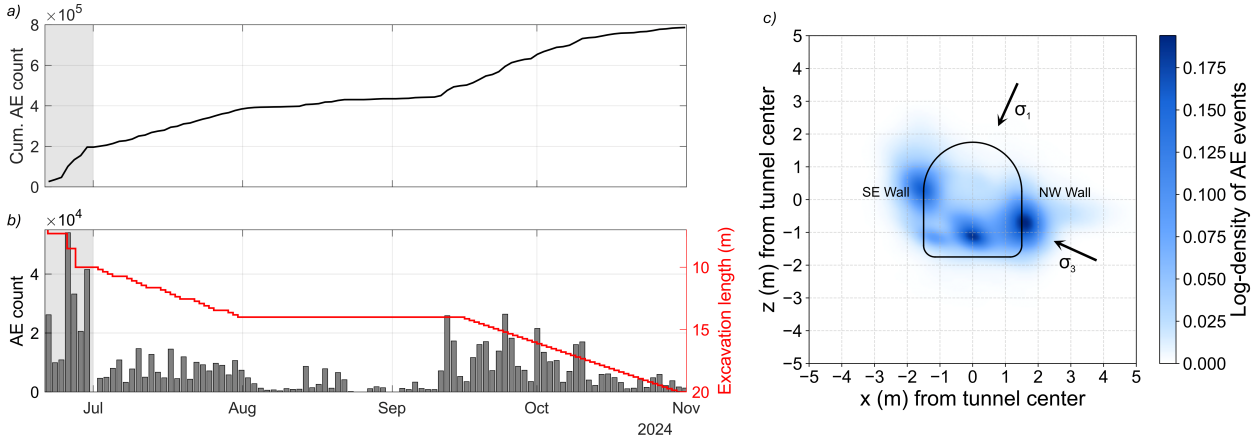


Figure 11: AE monitoring during PRECODE tunnel excavation: a) cumulative AE count during PRECODE excavation (shaded area indicates drill and blast excavation); b) AE count during PRECODE tunnel excavation with excavation lengths marked as red solid line; c) Log-density of AE events registered during the PRECODE tunnel excavation in an x-z plane. The ideal tunnel geometry is marked for reference.

6.2 Short-Term Development of Excavation Damage Zone around PRECODE Mine-by Tunnel

Upon completion of the PRECODE mine-by tunnel, a number of terrestrial laser scanning (TLS) and outbreak mapping activities were conducted to assess the characteristics of EDZ around the tunnel. Here, the term EDZ refers specifically to the excavation-induced damage manifested at the exposed tunnel surface and detected by laser scanning, including the observed HDZ and CDZ. The point clouds, with average point spacing of 2 mm, were acquired using terrestrial laser scanner (LiDAR, Optech Teledyne). All scans were registered together and characteristics of the EDZ including depth, shape and orientation were analyzed using the cloud-to-cloud distance algorithm in Cloud Compare software (CloudCompare, 2023), by comparing the current profile of the tunnel against the designed horseshoe-shaped tunnel.

Figure 12 shows the location and extent of short-term EDZ around the tunnel after completion of both PRECODE and FEAR Section in June 2025. The maximum extent of the brittle failure in the

form of spalling is approximately 60 cm and is concentrated in the lower NW wall (lower right) and the upper SE wall (upper left). The location of the EDZ concentration agrees with the seismic monitoring data, the overall understanding of the stress regime at the BedrettoLab (Ma et al., 2019; Bröker & Ma, 2022; Bröker et al., 2024) and the results of the stress modelling (Hamdi et al., 2025), where normal faulting is likely to be the background stress regime in the area of the PRECODE Section, with the principal stresses being slightly deviated from horizontality and verticality. The non-symmetrical formation of the EDZ also suggests that the trajectory of the tunnel is not parallel to one of the principal stresses. The location of the overbreaks and spalling developed in the characterization borehole (BPR_09 in Figure 6) drilled parallel to the trajectory of the tunnel also agreed with the spalling locations around the tunnel. The rock around the PRECODE Section is considered to be massive to moderately fractured rock mass with sporadic distribution of discontinuities. To differentiate stress-induced damage in intact rock from local structural overbreak, we complemented the TLS measurements with detailed field observations. What is also clearly observed is the interaction between the pre-existing fractures and the stress-induced fractures in some areas of the mine-by tunnel, an example being the slab failure in the SE wall at TM 20 and similar overbreak in the opposite wall (NW) (Figure 12). The comparison between the construction induced damage (CDZ) between D&B and LDRB area shows that the extent of the CDZ is approximately 15-20 cm higher in the D&B section as a result of the excavation method. It is also shown that the LDRB method is efficient in reducing the CDZ due to its minimal impact to the surrounding rocks.

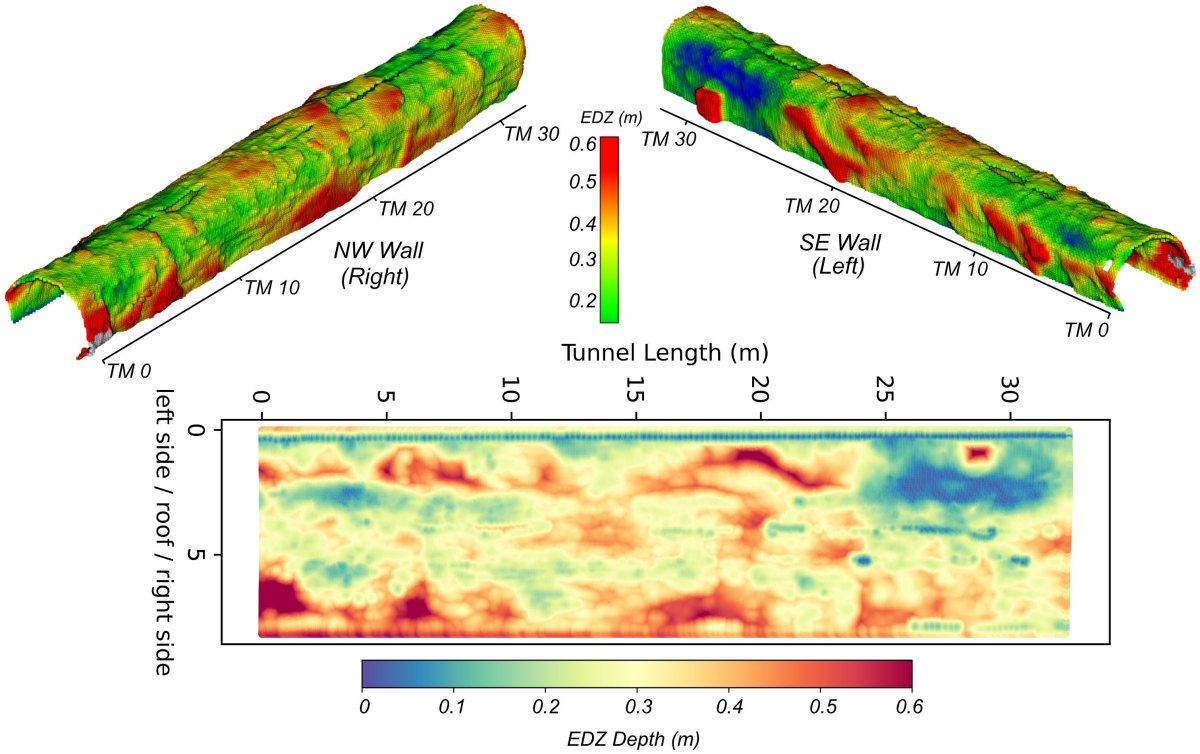


Figure 12: The calculated depth of EDZ around the PRECODE Tunnel obtained from TLS, Top: Isometric view of the EDZ depth on the 3D point clouds, Bottom: EDZ depth projected on the unwrapped PRECODE tunnel

6.3 Construction-Induced Damage

The electrical resistivity measurements collected along the PRECODE tunnel were examined to investigate how the excavation process, and subsequent damage of the rock mass due to different excavation method, may reflect in the electrical resistivity of the rock. Here, the

hypothesis is that an increased excavation damage zone may result in lower resistivity zones, because the granitic host rock is highly impermeable and therefore highly resistive. Any cracks in the rock will result in preferential flow paths, especially after the space between the cracks has been filled by water. Since the measurements shown below have been collected almost a year after the tunnel was excavated, we expect that saturation had taken place and the damaged zone will appear as less electrically resistive. ERT measurements are used to image the characteristics of the inner and outer EDZ zones and to assess the potential impact of the excavation method on their properties. The measurement process considered Wenner, Schlumberger and Dipole-Dipole electrode arrays for 31 electrodes in total. These electrodes span the drill and blast (first 16) and soft excavation (following 15) zones. The transition occurs in the middle of the profile, precisely at 1.5 m. The first electrode is denoted as the origin. To assess the precision of the campaign, we collect reciprocal measurements, where the current injection electrodes (A&B) are swapped with the potential measurement electrodes (M&N). Theory suggests that such a swapping should result in identical readings, unless the host rock behaves non-linearly or if there is a change in the medium (e.g., water infiltration or drying of the rock) occurring in the time between these two measurements (Parasnis, 1988). Regarding the latter, we do not expect any influence as these measurements were collected within a few hours. To obtain a geometry for the forward and inverse modeling of the electrical resistivity data, we used precise laser scanning information outlined in Section 6.2. From the laser scans we extracted the topography of the tunnel wall, and by determining where the electrodes lie, we extracted the geometry of the profile. The deviation from a flat topography is considerable; in some cases, up to 10 cm of topography is observed. It was therefore essential to account for the irregular shape of the tunnel wall when forward modeling the electrical response. For the subsequent modeling we only assume a 2D cross section. The inversion was run with ResIPy (Blanchy et al., 2020) on a triangular mesh, and convergence was reached after 10 iterations.

Figure 13 shows the comparison between the forward and reciprocal measurements for the profile. The scatter plot suggests that the measurements are highly correlated, especially for high resistance values, as expected for good repeatability (Tso et al., 2017). The second panel shows how the reciprocal error, defined as $\frac{|R_f - R_r|}{R_{av}}$ where the average resistance is computed from $R_{av} = \frac{(R_f + R_r)}{2}$. Here, R_f refers to the forward measurement and R_r refers to the reciprocal measurement. A total of 855 measurements are considered, and after filtering 527 measurements remain for the inversion. The observed apparent resistivity values, once inverted, span roughly 40-24,000 Ohm.m across the profile, with the bulk of the model falling between 450 and 2,200 Ohm.m (Figure 14). This range is consistent with granite in a fractured, moderately wet state rather than dry granite. Fu et al., (2024) report resistivities of ~2,200-5,600 Ohm.m for intact biotite/monzonitic granite core samples, and as low as ~20 Ohm.m for water-bearing fractured granite zones. Our observed range falls between these two references, consistent with an excavation damage zone that is fractured but not fully saturated. To our knowledge, this is the first ERT dataset collected across a controlled drill-and-blast/mechanical-excavation transition within an operating tunnel under near-identical geological and stress conditions, so a direct quantitative benchmark for the expected resistivity contrast between excavation methods is not available in the literature.

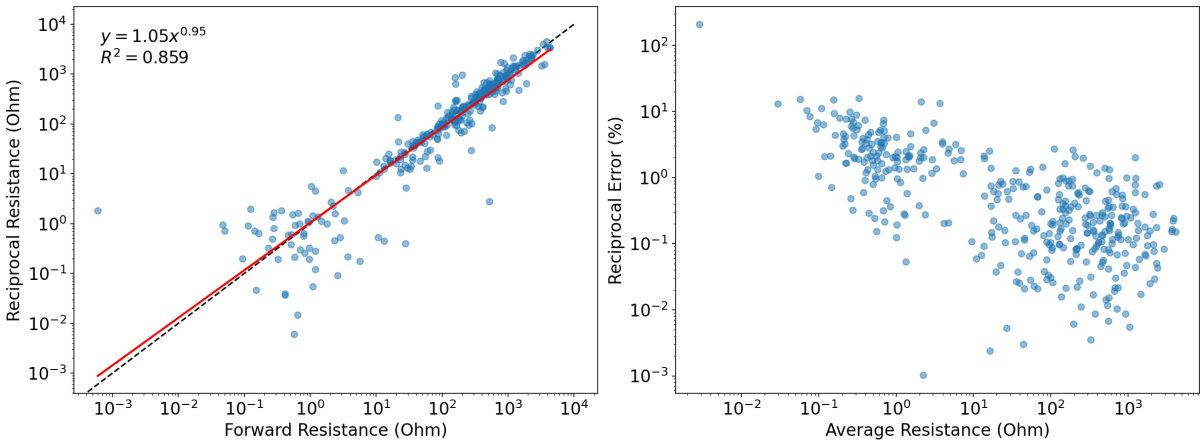


Figure 13: The length panel shows a comparison of forward and reciprocal electrical resistivity measurements for the profile under examination, alongside the perfect match line. The forward and reciprocal measurements overlap well, especially for high resistivities, suggesting high precision. The right panel shows the reciprocal error compared to the average resistance for the measurements. Reciprocal errors above 10% are not included in the data inversion.

The results of the inversion are presented in Figure 14. Overall, higher resistivities are observed in the soft excavation region compared to the D&B part, aligning with the initial hypothesis that the soft excavation keeps the rock intact and therefore results in higher electrical resistance. A high resistivity zone in the initial section of the drill and blast section may correlate with a block of intact rock. In addition, the very high resistivity sections on the surface of the inversion mesh, at 0.5 m and 2.6 m, may be related to bad coupling of electrodes or loose parts of the rock that do not couple well to the remaining rock mass.

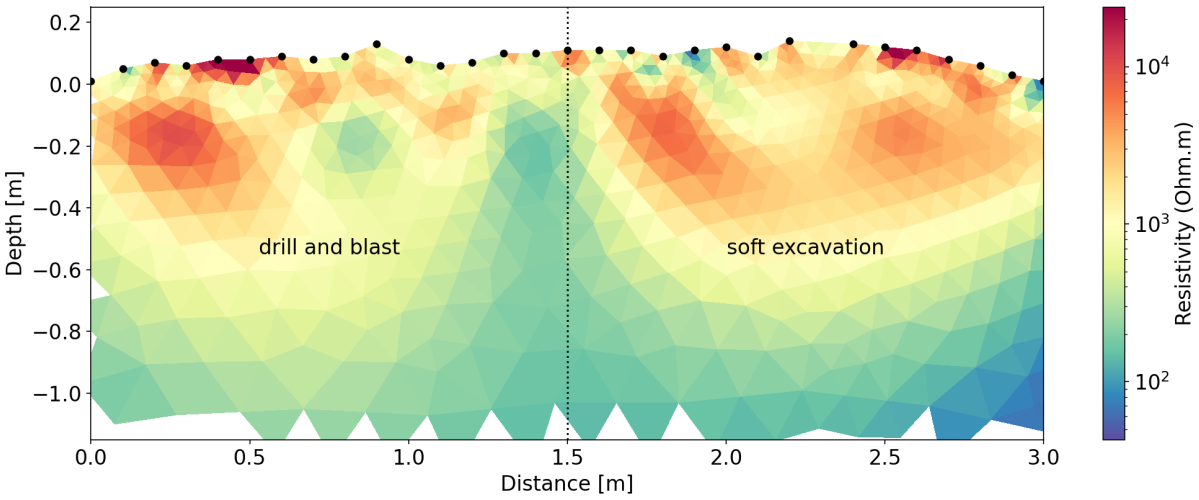


Figure 14: Inversion results for electrical resistivity tomography spanning the drill and blast, and soft excavation zones. The results show some prominent very high resistivity zones in the shallow few centimeters, likely resulting from loose slabs of rock along the wall. The information at depth reveals a higher resistivity zone for the soft excavation, suggesting more intact rock compared to the drill and blast zone.

7. Discussion

7.1 Influence of Excavation Method on Brittle Damage

The preliminary PRECODE results provide field-scale evidence that the excavation method influences both the intensity of excavation-induced microcracking and the resulting surface damage. The AE monitoring shows substantially greater activity during D&B excavation than

during LDRB. When normalized by excavation length, the AE activity was approximately 72,717 events per meter for the D&B section, compared with 46,664 and 48,232 events per meter for the two LDRB sections. The D&B section exhibited approximately 50–55% higher AE activity per meter of excavation. This is consistent with observations from similar URLs where a significantly higher degree of fracturing and AE events were recorded during D&B excavation in comparison with TBM (Falls & Young, 1998; Siren et al., 2015). This can be attributed to additional dynamic loading associated with blasting, which acts in addition to the stress redistribution caused by tunnel excavation. TLS data indicates that the extent of the construction-induced damage zone (CDZ) is approximately 15–20 cm greater in the D&B section than in the LDRB section. The higher electrical resistivity observed in the LDRB section further suggests that a greater proportion of the rock mass remains intact compared with the D&B section. Together, these observations indicate that reducing excavation-induced disturbance can reduce both the surface damage and the microcracking response of the surrounding rock mass.

7.2 Surface Expression of Damage and the Subsurface EDZ

The combined AE and TLS observations highlight an important distinction between the visible surface expression of excavation damage and the subsurface EDZ. TLS measurements provide detailed information on the geometry and extent of spalling and overbreak at the exposed tunnel surface. The maximum spalling depth observed in the PRECODE tunnel is approximately 0.6 m, whereas the spatial distribution of AE activity extends to approximately 1.5 m from the tunnel wall. The observed distribution is also consistent with the conceptual distinction between the highly damaged near-surface region and the surrounding zone of more distributed microcracking. The highest AE concentration within approximately 0.5–0.6 m of the tunnel wall broadly corresponds to the region in which pronounced surface damage is observed, while lower-density AE activity extends further into the rock mass. This transition is gradual rather than defined by a sharp boundary. Multi-disciplinary monitoring methods can help resolve the different zones of excavation-induced damage. Surface scanning is particularly effective for quantifying spalling, overbreak and surface morphology, whereas AE monitoring provides information on subsurface microcracking. Hydraulic and geophysical measurements provide additional information on changes in fracture connectivity and potential permeability enhancement.

7.3 Implications for Time-Dependent EDZ Evolution

The PRECODE observations further demonstrate that excavation-induced damage cannot be interpreted independently of the geological and stress conditions. The asymmetric distribution of AE activity and surface spalling is consistent with the measured and modelled stress field at BedrettoLab, where the principal stresses are not perfectly aligned with the tunnel axis. This observation is particularly relevant for crystalline repository host rocks, which may appear relatively massive at the tunnel scale while still containing pre-existing fractures. Such structures can locally modify stress concentrations and provide preferential locations for fracture initiation and propagation. A potential interaction of pre-existing fractures and newly-generated stress-induced fractures over time may further enhance the permeability and compromise the integrity of the DGR infrastructures. The continued in-situ monitoring provides a basis for determining how the short-term damage evolves over time and how changes in fracture development are coupled with the hydraulic and mechanical properties of the surrounding rock mass.

8. Conclusion and Outlook

The BedrettoLab was established in the Swiss Central Alps within the old Bedretto Tunnel. The facility hosts a wide range of meso- to hectometer-scale experiments addressing key challenges related to geothermal energy, induced seismicity, and deep geological disposal of nuclear waste.

The PRECODE mine-by experiment at BedrettoLab builds upon insights gained from existing URLs to advance our understanding of time-dependent brittle fracturing in crystalline rocks relevant to the disposal of heat-generating nuclear waste. By combining investigations of the mature EDZ in the Bedretto Tunnel with intensive, multidisciplinary monitoring of EDZ development around the PRECODE tunnel, a unique opportunity is created to study the spatial and temporal evolution of the EDZ under natural repository conditions.

Within the PRECODE project, a new 100 m long mine-by tunnel was excavated between 2024 and 2025 as a branch of the existing Bedretto Tunnel at an overburden depth of approximately 1300 m. The high in-situ stresses associated with this overburden were sufficient to induce brittle fracturing in the form of spalling. To capture the development of the Excavation Damage Zone (EDZ), the tunnel surroundings were densely instrumented before and during excavation using a multidisciplinary monitoring system comprising active and passive seismic monitoring, hydraulic monitoring, deformation monitoring using Fiber Bragg Grating (FBG) and Distributed Strain Sensing (DSS), as well as geophysical monitoring through electrical resistivity tomography (ERT) and ground-penetrating radar (GPR). In addition, two excavation methods: controlled drill-and-blast (D&B) and line drilling and rock breaking (LDRB) were employed to evaluate the influence of excavation-induced damage on EDZ development. The comparison between the LDRB and D&B sections provides a unique opportunity to distinguish between damage resulting primarily from stress redistribution and damage associated with both stress redistribution and excavation-induced disturbance, thereby improving our understanding of the mechanisms governing EDZ formation and evolution in crystalline rocks.

Acoustic emission (AE) monitoring revealed significantly higher AE activity during the D&B phase than during excavation using the LDRB method, indicating a greater degree of excavation-induced damage associated with drill-and-blast excavation. A pronounced concentration of AE events was observed along the tunnel sidewalls, where stress concentrations were highest. The spatial distribution of AE activity suggests that the maximum principal stress, likely corresponding to the vertical stress component at the PRECODE site, is inclined by approximately 15° relative to the vertical. Systematic AE events were located within approximately 1.5 m of the tunnel wall, which likely represents the maximum extent of the outer EDZ. The highest event density was concentrated within the first 0.5–0.6 m from the tunnel wall, corresponding to the zone of visible surface damage, including the CDZ and HDZ. These findings are consistent with observations from terrestrial laser scanning and geophysical monitoring using ERT. The ERT inversions indicate higher electrical resistivities in the LDRB section compared to the D&B section, supporting the hypothesis that the LDRB method reduces excavation-induced damage and preserve a greater degree of rock mass integrity.

The proximity of the PRECODE mine-by tunnel to the FEAR project, in which a natural fault zone will be stimulated under controlled conditions, provides a unique opportunity to investigate the impact of fault activation and induced seismicity on tunnel stability and EDZ evolution. Furthermore, PRECODE offers an exceptional framework for bridging laboratory and in-situ observations, particularly in improving the characterization of subcritical and time-dependent crack growth processes and their implications for long-term barrier integrity. Ongoing laboratory experiments, including fatigue, relaxation, and fracture mechanics tests conducted under controlled environmental conditions, will provide valuable insight into the long-term behavior of Rotondo Granite and the mechanisms governing stress corrosion and progressive damage accumulation. In parallel, the comparison of hydraulic properties measured within the mature (>40-year-old) EDZ of the Bedretto Tunnel and the newly excavated PRECODE tunnel will enable quantification of long-term permeability evolution under natural environmental perturbations.

Together, these investigations will contribute to a more comprehensive understanding of the spatial and temporal evolution of excavation-induced damage in crystalline rocks and provide critical data for improving predictive models and long-term safety assessments of deep geological repositories for heat-generating nuclear waste.

Code and Data Availability

The tunnel geometry data, including high-resolution point clouds, surface meshes, and borehole information, are publicly available through the ETH data repository at ETH Research Collection Dataset (https://doi.org/10.3929/ethz-c-000801363). Additional raw and processed datasets generated and analyzed during this study are available from the corresponding author upon reasonable request.

Author Contributions

This collective work has been carried out under umbrella of the PRECODE Project and authors have contributed to different part of the manuscript. Specifically, PH, JD, MK, APR, LV, AS, PB, PA conducted the mechanical, hydrogeological, seismological, geophysical and geological characterization, data collection and analysis. MP, SG, YG, SM carried out the laboratory testing and analysis. KB and XM carried out the stress measurement and analysis. NB and KK provided support in the numerical modelling part. PS, VD, MJ, AZ contributed to the design and installation of the in-situ monitoring. MH and MW oversaw the operational and logistical aspects of the experiments. FA, SW supervised the project. All co-authors contributed to the writing of the paper.

Competing interests.

The contact author has declared that neither they nor their co-authors have any competing interests.

Funding

The PRECODE project is funded by the by German's Federal Agency for Radioactive Waste Disposal (BGE), Research Order Number: STAFuE-21-07-Klei. The BedrettoLab is financed by the Werner Siemens Foundation, ETH Zürich, and the Swiss National Science Foundation.

References

Achtziger-Zupančič, P., Ceccato, A., Zappone, A. S., Pozzi, G., Shakas, A., Amann, F., Behr, W. M., Escallon Botero, D., Giardini, D., Hertrich, M., Jalali, M., Ma, X., Meier, M.-A., Osten, J., Wiemer, S., & Cocco, M. (2024). Selection and Characterisation of the Target Fault for Fluid-Induced Activation and Earthquake Rupture Experiments. *EGUsphere*, 1–38. https://doi.org/10.5194/egusphere-2024-586

Alcaino-Olivares, R., Paraskevopoulou, C., & Perras, M. A. (2024). Assessing Long-Term Excavation Damage in Switzerland's Bedretto Adit: A Field Investigation in the Northern

Section. *Geotechnical and Geological Engineering*. https://doi.org/10.1007/s10706-023-02735-8

Amann, F., Button, E. A., Evans, K. F., Gischig, V. S., & Blümel, M. (2011). Experimental Study of the Brittle Behavior of Clay shale in Rapid Unconfined Compression. *Rock Mechanics and Rock Engineering*, *44*(4), 415–430. https://doi.org/10.1007/s00603-011-0156-3

Andersson, J. C., & Martin, C. D. (2009). The Äspö pillar stability experiment: Part I—Experiment design. *International Journal of Rock Mechanics and Mining Sciences*, *46*(5), 865–878. https://doi.org/10.1016/j.ijrmms.2009.02.010

Andersson, J. C., Martin, C. D., & Stille, H. (2009). The Äspö Pillar Stability Experiment: Part II—Rock mass response to coupled excavation-induced and thermal-induced stresses. *International Journal of Rock Mechanics and Mining Sciences*, *46*(5), 879–895. https://doi.org/10.1016/j.ijrmms.2009.03.002

Atkinson, B. K. (1984). Subcritical crack growth in geological materials. *Journal of Geophysical Research: Solid Earth*, *89*(B6), 4077–4114. https://doi.org/10.1029/JB089iB06p04077

Bäckblom, G., & Martin, C. D. (1999). Recent experiments in hard rocks to study the excavation response: Implications for the performance of a nuclear waste geological repository. *Tunnelling and Underground Space Technology*, *14*(3), 377–394. https://doi.org/10.1016/S0886-7798(99)00053-X

Bianchi, P., Selvadurai, P. A., Dal Zilio, L., Salazar Vásquez, A., Madonna, C., Gerya, T., & Wiemer, S. (2024). Pre-Failure Strain Localization in Siliclastic Rocks: A Comparative Study of Laboratory and Numerical Approaches. *Rock Mechanics and Rock Engineering*, *57*(8), 5371–5395. https://doi.org/10.1007/s00603-024-04025-y

Bieniawski, Z. T. (1967a). *Mechanism of brittle fracture of rock*. 14.

Bieniawski, Z. T. (1967b). Mechanism of brittle fracture of rock: Part I—theory of the fracture process. *International Journal of Rock Mechanics and Mining Sciences & Geomechanics Abstracts*, *4*(4), 395–406. https://doi.org/10.1016/0148-9062(67)90030-7

1005 Blanchy, G., Saneiyan, S., Boyd, J., McLachlan, P., & Binley, A. (2020). ResIPy, an intuitive open
1006 source software for complex geoelectrical inversion/modeling. *Computers &*
1007 *Geosciences*, *137*, 104423. https://doi.org/10.1016/j.cageo.2020.104423
1008 Bossart, P., Bernier, F., Birkholzer, J., Bruggeman, C., Connolly, P., Dewonck, S., Fukaya, M.,
1009 Herfort, M., Jensen, M., Matray, J.-M., Mayor, J. C., Moeri, A., Oyama, T., Schuster, K.,
1010 Shigeta, N., Vietor, T., & Wieczorek, K. (2017). Mont Terri rock laboratory, 20 years of
1011 research: Introduction, site characteristics and overview of experiments. *Swiss Journal of*
1012 *Geosciences*, *110*(1), 3–22. https://doi.org/10.1007/s00015-016-0236-1
1013 Bossart, P., Meier, P. M., Moeri, A., Trick, T., & Mayor, J.-C. (2002). Geological and hydraulic
1014 characterisation of the excavation disturbed zone in the Opalinus Clay of the Mont Terri
1015 Rock Laboratory. *Engineering Geology*, *66*(1–2), 19–38. Scopus.
1016 https://doi.org/10.1016/S0013-7952(01)00140-5
1017 Brantut, N., Heap, M. J., Meredith, P. G., & Baud, P. (2013). Time-dependent cracking and brittle
1018 creep in crustal rocks: A review. *Journal of Structural Geology*, *52*, 17–43.
1019 https://doi.org/10.1016/j.jsg.2013.03.007
1020 Bröker, K., & Ma, X. (2022). Estimating the Least Principal Stress in a Granitic Rock Mass:
1021 Systematic Mini-Frac Tests and Elaborated Pressure Transient Analysis. *Rock Mechanics*
1022 *and Rock Engineering*, *55*(4), 1931–1954. https://doi.org/10.1007/s00603-021-02743-1
1023 Bröker, K., Ma, X., Zhang, S., Gholizadeh Doonechaly, N., Hertrich, M., Klee, G., Greenwood, A.,
1024 Caspari, E., & Giardini, D. (2024). Constraining the Stress Field and its Variability at the
1025 Bedrettolab: Elaborated Hydraulic Fracture Trace Analysis. *International Journal of Rock*
1026 *Mechanics and Mining Sciences*, *178*, 105739.
1027 https://doi.org/10.1016/j.ijrmms.2024.105739
1028 Cai, M., Kaiser, P. K., Tasaka, Y., Maejima, T., Morioka, H., & Minami, M. (2004). Generalized crack
1029 initiation and crack damage stress thresholds of brittle rock masses near underground
1030 excavations. *International Journal of Rock Mechanics and Mining Sciences*, *41*(5), 833–
1031 847. https://doi.org/10.1016/j.ijrmms.2004.02.001

1032 Cappa, F., & Rutqvist, J. (2011). Modeling of coupled deformation and permeability evolution
1033 during fault reactivation induced by deep underground injection of CO2. *International*
1034 *Journal of Greenhouse Gas Control*, *5*(2), 336–346.
1035 https://doi.org/10.1016/j.ijggc.2010.08.005
1036 Ceccato, A., Behr, W. M., Zappone, A. S., Tavazzani, L., & Giuliani, A. (2024). Structural Evolution,
1037 Exhumation Rates, and Rheology of the European Crust During Alpine Collision:
1038 Constraints From the Rotondo Granite—Gotthard Nappe. *Tectonics*, *43*(6),
1039 e2023TC008219. https://doi.org/10.1029/2023TC008219
1040 Ceccato, A., Hinshaw, E., Behr, W. M., Zappone, A. S., & Giardini, D. (2026). 3D geologic modeling
1041 for digital twin applications: Insights from the Bedretto Underground Laboratory. *Swiss*
1042 *Journal of Geosciences*, *119*, 33–48. https://doi.org/10.3897/sjg.119.181128
1043 Chen, H., Selvadurai, P. A., de Geus, T., Salazar Vásquez, A. F., Bianchi, P., Michail, S., Rast, M.,
1044 Madonna, C., & Wiemer, S. (2025). Investigating Criticality in Rock Failure Using Fiber-
1045 Optic Strain Sensing. *Geophysical Research Letters*, *52*(14), e2025GL115010.
1046 https://doi.org/10.1029/2025GL115010
1047 CloudCompare. (2023). *CloudCompare 32.12 [GPL Software]* [Computer software].
1048 https://www.cloudcompare.org/ (accessed on 15 August 2023).
1049 Collins, D. S. (1997). *Excavation induced seismicity in granite rock: A case study at the*
1050 *underground research laboratory, Canada*. [Ph.D., University of Keele].
1051 https://ethos.bl.uk/OrderDetails.do?uin=uk.bl.ethos.389605
1052 Cook, N. G. W. (1965). The failure of rock. *International Journal of Rock Mechanics and Mining*
1053 *Sciences & Geomechanics Abstracts*, *2*(4), 389–403. https://doi.org/10.1016/0148-
1054 9062(65)90004-5
1055 Damjanac, B., & Fairhurst, C. (2010). Evidence for a Long-Term Strength Threshold in Crystalline
1056 Rock. *Rock Mechanics and Rock Engineering*, *43*(5), 513–531.
1057 https://doi.org/10.1007/s00603-010-0090-9

David, C., Nejati, M., & Geremia, D. (2020). *On petrophysical and geomechanical properties of Bedretto Granite* [Report]. ETH Zurich. https://doi.org/10.3929/ethz-b-000428267

Diederichs, M. (2003). Manuel Rocha Medal Recipient Rock Fracture and Collapse Under Low Confinement Conditions. *Rock Mechanics and Rock Engineering*, *36*(5), 339–381. https://doi.org/10.1007/s00603-003-0015-y

Diederichs, M. S. (2007). The 2003 Canadian Geotechnical Colloquium: Mechanistic interpretation and practical application of damage and spalling prediction criteria for deep tunnelling. *Canadian Geotechnical Journal*, *44*(9), 1082–1116. https://doi.org/10.1139/T07-033

Diederichs, M. S., Carter, T. G., & Martin, C. D. (2010). Practical rock spall prediction in tunnels. *In Proceedings of the World Tunnel Congress 2010, Paper No 517*.

Diederichs, M. S., Kaiser, P. K., & Eberhardt, E. (2004). Damage initiation and propagation in hard rock during tunnelling and the influence of near-face stress rotation. *International Journal of Rock Mechanics and Mining Sciences*, *41*(5), 785–812. https://doi.org/10.1016/j.ijrmms.2004.02.003

Dutler, N., Nejati, M., Valley, B., Amann, F., & Molinari, G. (2018). On the link between fracture toughness, tensile strength, and fracture process zone in anisotropic rocks. *Engineering Fracture Mechanics*, *201*, 56–79. https://doi.org/10.1016/j.engfracmech.2018.08.017

Eberhardt, E. (1998). *Brittle rock fracture and progressive damage in uniaxial compression*. *Ph.D. thesis, Department of Geological Sciences, University of Saskatchewan, Saskatoon*. http://library.usask.ca/theses/available/etd-10212004-001228/

Eberhardt, E., Stead, D., & Stimpson, B. (1999). Quantifying progressive pre-peak brittle fracture damage in rock during uniaxial compression. *International Journal of Rock Mechanics and Mining Sciences*, *36*(3), 361–380. https://doi.org/10.1016/S0148-9062(99)00019-4

Falls, S. D., & Young, R. P. (1998). Acoustic emission and ultrasonic-velocity methods used to characterise the excavation disturbance associated with deep tunnels in hard rock. *Tectonophysics*, *289*(1), 1–15. https://doi.org/10.1016/S0040-1951(97)00303-X

1085 Faulkner, D. R., Jackson, C. A. L., Lunn, R. J., Schlische, R. W., Shipton, Z. K., Wibberley, C. A. J.,
1086 & Withjack, M. O. (2010). A review of recent developments concerning the structure,
1087 mechanics and fluid flow properties of fault zones. *Journal of Structural Geology, Fault*
1088 *Zones*, *32*(11), 1557–1575. https://doi.org/10.1016/j.jsg.2010.06.009
1089 Frieg, B., Albert, W., Blaser, P. C., Adams, J., Dollinger, H., Kuhlmann, U., & Lanyon, G. W. (2012).
1090 *Grimsel test site. Excavation disturbed zone experiment (EDZ)*.
1091 https://www.osti.gov/etdeweb/biblio/22640026
1092 Fu, Z., Zhang, Y., Ji, H., Zhang, C., Chen, D., & Qin, Y. (2024). Characteristics of resistivity variation
1093 in deep granite and in-situ detection applications. *Scientific Reports*, *14*(1), 6120.
1094 https://doi.org/10.1038/s41598-024-56695-x
1095 Hafner, S. (1958). *Petrographie des südwestlichen Gotthardmassivs zwischen St.Gotthardpass*
1096 *und Nufenenpass* [Doctoral Thesis, ETH Zurich]. https://doi.org/10.3929/ethz-a-
1097 000097546
1098 Hajiabdolmajid, V., Kaiser, P. K., & Martin, C. D. (2002). Modelling brittle failure of rock.
1099 *International Journal of Rock Mechanics and Mining Sciences*, *39*(6), 731–741.
1100 https://doi.org/10.1016/S1365-1609(02)00051-5
1101 Hamdi, P., Achtziger, P., Dickmann, J., Kruszewski, M., Rinaldi, A. P., Villiger, L., Shakas, A.,
1102 Perras, M., Bahrani, N., Jiang, D., Amann, F., & Wiemer, S. (2024, June 23). *Progressive*
1103 *Excavation Disturbance Zone Evolution During and Post Mine-By Tunneling (PRECODE) –*
1104 *Insight into a New Underground Research Laboratory for Crystalline Rocks in the*
1105 *BedrettoLab*. 58th U.S. Rock Mechanics/Geomechanics Symposium.
1106 https://doi.org/10.56952/ARMA-2024-0543
1107 Hamdi, P., Herzog, A., Dickmann, J., Lemaire, E., Perras, L., & Amann, F. (2026). *Environmental*
1108 *Effects on Sub-Critical Crack Growth and Stress Corrosion in Rotondo Granite from*
1109 *BedrettoLab, Switzerland*. 60th U.S. Rock Mechanics/Geomechanics Symposium.
1110 Hamdi, P., Stead, D., & Elmo, D. (2015). Characterizing the influence of stress-induced
1111 microcracks on the laboratory strength and fracture development in brittle rocks using a

finite-discrete element method-micro discrete fracture network FDEM-μDFN approach. *Journal of Rock Mechanics and Geotechnical Engineering*, *7*(6), 609–625. https://doi.org/10.1016/j.jrmge.2015.07.005

Hamdi, P., Stead, D., & Elmo, D. (2017, June 25). *A Review of the Application of Numerical Modelling in the Prediction of Depth of Spalling Damage Around Underground Openings*. 51st U.S. Rock Mechanics/Geomechanics Symposium. https://dx.doi.org/

Hamdi, P., Ufrecht, S., Achtziger-Zupančič, P., Bröker, K., Ma, X., & Amann, F. (2025). Understanding the Regional Stress in Active Tectonic Regime Using 3D Numerical Modeling, Case Study of BedrettoLab, Switzerland. *Rock Mechanics and Rock Engineering*. https://doi.org/10.1007/s00603-025-04740-0

Hegger, S., Vlachopoulos, N., Poles, T., & Diederichs, M. S. (2022). Measuring the Full-Field Strain Response of Uniaxial Compression Test Specimens Using Distributed Fiber Optic Sensing. *Rock Mechanics and Rock Engineering*, *55*(5), 2615–2630. https://doi.org/10.1007/s00603-021-02643-4

Helmholtz-Centre Potsdam-GFZ German Research Centre For Geosciences & GEMPA GmbH. (2008). *The SeisComP seismological software package* [Computer software]. GFZ Data Services. https://doi.org/10.5880/GFZ.2.4.2020.003

Hoek, E. (1968). *Brittle fracture of rock, Chapter 4 in rock mechanics in engineering practice, London: J. Wiley, 99 to 124, Edited by K.G. Stagg and O.C. Zienkiewicz*. www.rocscience.com/hoek/references/H1968a.pdf

Hoek, E., & Bieniawski, Z. T. (1965). Brittle fracture propagation in rock under compression. *International Journal of Fracture Mechanics*, *1*(3), 137–155. https://doi.org/10.1007/BF00186851

Horii, H., & Nemat-Nasser, S. (1985). Compression-induced microcrack growth in brittle solids: Axial splitting and shear failure. *Journal of Geophysical Research: Solid Earth*, *90*(B4), 3105–3125. https://doi.org/10.1029/JB090iB04p03105

Huber, B. (2004). *Stress-induced Fractures in the Deep-seated Bedretto Tunnel: Their Geological and Geomechanical Reasons* [Diploma dissertation]. ETH Zurich.

Jonsson, M., Baeckstroem, A., Feng, Q., Berglund, J., Johansson, M., Mas Ivars, D., & Olsson, M. (2009). *Aespoe Hard Rock Laboratory. Studies of factors that affect and controls the Excavation Damaged/Disturbed Zone*. https://www.osti.gov/etdeweb/biblio/968893

Jordan, D. (2019). *Geological Characterization of the Bedretto Underground Laboratory for Geoenergies* [Master Thesis, ETH Zurich, Geological Institute]. https://doi.org/10.3929/ethz-b-000379305

Kaiser, P. K., Amann, F., & Steiner, W. (2010, June 15). *How Highly Stressed Brittle Rock Failure Impacts Tunnel Design*. ISRM International Symposium - EUROCK 2010. https://www.onepetro.org/conference-paper/ISRM-EUROCK-2010-003

Kaiser, P. K., & Kim, B. H. (2008). *Rock mechanics challenges in underground construction and mining, keynote lecture, Proceedings 1st SHIRMS, South Hemisphere International Rock Mechanics Symposium (Perth, Australia, September 2008), Vol. 1, pp. 23-38.*

Kaiser, P., McCreath, D., & Tannant, D. (1996). *Canadian Rockburst Support Handbook*. Geomechanics Research Centre.

Keller, F., & Schneider, T. R. (1982). Geologie und Geotechnik. *Schweizer Ingenieur Und Architekt*, *100*(24), 512. https://doi.org/10.5169/seals-74820

Kelsall, P. C., Case, J. B., & Chabannes, C. R. (1984). Evaluation of excavation-induced changes in rock permeability. *International Journal of Rock Mechanics and Mining Sciences & Geomechanics Abstracts*, *21*(3), 123–135. https://doi.org/10.1016/0148-9062(84)91530-4

Kranz, R. L. (1983). Microcracks in rocks: A review. *Tectonophysics, Continental Tectonics: Structure, Kinematics and Dynamics*, *100*(1), 449–480. https://doi.org/10.1016/0040-1951(83)90198-1

Kruszewski, M., Hamdi, P., Dickmann, J., Amann, F., Villiger, L., Bianchi, P., Rinaldi, A. P., Wiemer, S., & Perras, M. (2026, June 21). *Crack Initiation of Rotondo Granite during the PRECODE*

Mine-by Experiment in the BedrettoLab. 60th U.S. Rock Mechanics/Geomechanics Symposium. https://doi.org/10.56952/ARMA-2026-0091

Labhart, T. (2005). *Erläuterungen Zum Geologischen Atlas Des Schweiz 1:25000, Val Bedretto, Atlasblatt 68*. [Map].

Li, M., Zuo, J., Hu, D., Shao, J., & Liu, D. (2020). Experimental and numerical investigation of microstructure effect on the mechanical behavior and failure process of brittle rocks. *Computers and Geotechnics*, *125*, 103639. https://doi.org/10.1016/j.compgeo.2020.103639

Li, Y., & Bahrani, N. (2021). Strength and failure mechanism of highly interlocked jointed pillars: Insights from upscaled continuum grain-based models of a jointed rock mass analogue. *Computers and Geotechnics*, *137*, 104278. https://doi.org/10.1016/j.compgeo.2021.104278

Li, Y., Yang, J., & Gao, X. (2025). Fault slip amplification mechanisms in deep mining due to heterogeneous geological layers. *Engineering Failure Analysis*, *169*, 109155. https://doi.org/10.1016/j.engfailanal.2024.109155

Lisjak, A., Garitte, B., Grasselli, G., Müller, H. R., & Vietor, T. (2015). The excavation of a circular tunnel in a bedded argillaceous rock (Opalinus Clay): Short-term rock mass response and FDEM numerical analysis. *Tunnelling and Underground Space Technology*, *45*, 227–248. https://doi.org/10.1016/j.tust.2014.09.014

Lockner, D. A., Byerlee, J. D., Kuksenko, V., Ponomarev, A., & Sidorin, A. (1991). Quasi-static fault growth and shear fracture energy in granite. *Nature*, *350*(6313), 39–42. https://doi.org/10.1038/350039a0

Lützenkirchen, V. H. (2002). *Structural geology and hydrogeology of brittle fault zones in the central and eastern Gotthard massif, Switzerland*. ETH Zurich.

Lützenkirchen, V., & Loew, S. (2011). Late Alpine brittle faulting in the Rotondo granite (Switzerland): Deformation mechanisms and fault evolution. *Swiss Journal of Geosciences*, *104*(1), 31–54. https://doi.org/10.1007/s00015-010-0050-0

Ma, X., Doonechaly, N. G., Hertrich, M., Gischig, V., & Klee, G. (2019). Preliminary in situ stress and fracture characterization in the Bedretto Underground Laboratory, Swiss Alps: Implications on hydraulic stimulation. In *Rock Mechanics for Natural Resources and Infrastructure Development—Full Papers*. CRC Press.

Ma, X., Hertrich, M., Amann, F., Bröker, K., Gholizadeh Doonechaly, N., Gischig, V., Hochreutener, R., Kästli, P., Krietsch, H., Marti, M., Nägeli, B., Nejati, M., Obermann, A., Plenkers, K., Rinaldi, A. P., Shakas, A., Villiger, L., Wenning, Q., Zappone, A., … Giardini, D. (2022). Multi-disciplinary characterizations of the BedrettoLab – a new underground geoscience research facility. *Solid Earth*, *13*(2), 301–322. https://doi.org/10.5194/se-13-301-2022

Martin, C. D. (1993). *The strength of massive Lac du Bonnet granite around underground openings*. University of Manitoba.

Martin, C. D. (1997). Seventeenth Canadian Geotechnical Colloquium: The effect of cohesion loss and stress path on brittle rock strength. *Canadian Geotechnical Journal*, *34*(5), 698–725.

Martin, C. D., & Chandler, N. A. (1994). The progressive fracture of Lac du Bonnet granite. *International Journal of Rock Mechanics and Mining Sciences & Geomechanics Abstracts*, *31*(6), 643–659. https://doi.org/10.1016/0148-9062(94)90005-1

Martin, C. D., & Christiansson, R. (2009). Estimating the potential for spalling around a deep nuclear waste repository in crystalline rock. *International Journal of Rock Mechanics and Mining Sciences*, *46*(2), 219–228. https://doi.org/10.1016/j.ijrmms.2008.03.001

Martin, C. D., Kaiser, P. K., & McCreath, D. R. (1999). Hoek-Brown Parameters for Predicting the Depth of Brittle Failure Around Tunnels. *Canadian Geotechnical Journal*, *36*(1), 136–151. Scopus. https://doi.org/10.1139/t98-072

Martin, C. D., Read, R. S., & Martino, J. B. (1997). Observations of brittle failure around a circular test tunnel. *International Journal of Rock Mechanics and Mining Sciences*, *34*(7), 1065–1073. https://doi.org/10.1016/S1365-1609(97)90200-8

1219 Martino, J. B., Dixon, D. A., Kozak, E. T., Gascoyne, M., Vignal, B., Sugita, Y., Fujita, T., &
1220 Masumoto, K. (2007). The tunnel sealing experiment: An international study of full-scale
1221 seals. *Physics and Chemistry of the Earth, Parts A/B/C, Clay in Natural and Engineered*
1222 *Barriers for Radioactive Waste Confinement - Part 1*, *32*(1), 93–107.
1223 https://doi.org/10.1016/j.pce.2006.04.023
1224 Meier, M.-A., Selvadurai, P., Gischig, V., Hertrich, M., Tinti, E., Rinaldi, A. P., Jalali, M., Spagnuolo,
1225 E., Zappone, A., Zilio, L. D., Pozzi, G., Massin, F., Ceccato, A., Shakas, A., Achtziger-
1226 Zupančič, P., Aretusini, S., Becattini, V., Behnen, K., Bröker, K., … Giardini, D. (2026).
1227 Activating a Natural Fault Zone in the Swiss Alps. *Seismica*, *5*(1).
1228 https://doi.org/10.26443/seismica.v5i1.2065
1229 Mellanen, S., Lehtimaeki, T., Heikkinen, E., Mustonen, S., & Norokallio, J. (2010). *EDZ09 project*
1230 *and related EDZ studies in ONKALO 2008-2010*.
1231 https://www.osti.gov/etdeweb/biblio/22134720
1232 Munjiza, A. (2004). *The Combined Finite-Discrete Element Method*. Wiley, Chichester, West
1233 Sussex, Hoboken. http://onlinelibrary.wiley.com/book/10.1002/0470020180
1234 Nara, Y. (2015). Effect of Anisotropy on the Long-Term Strength of Granite. *Rock Mechanics and*
1235 *Rock Engineering*, *48*(3), 959–969. https://doi.org/10.1007/s00603-014-0634-5
1236 Nara, Y., Hiroyoshi, N., Yoneda, T., & Kaneko, K. (2010). Effects of relative humidity and
1237 temperature on subcritical crack growth in igneous rock. *International Journal of Rock*
1238 *Mechanics and Mining Sciences*, *47*(4), 640–646.
1239 https://doi.org/10.1016/j.ijrmms.2010.04.009
1240 Nara, Y., & Kaneko, K. (2006). Sub-critical crack growth in anisotropic rock. *International Journal*
1241 *of Rock Mechanics and Mining Sciences*, *43*(3), 437–453.
1242 https://doi.org/10.1016/j.ijrmms.2005.07.008
1243 Nara, Y., Takada, M., Mori, D., Owada, H., Yoneda, T., & Kaneko, K. (2010). Subcritical crack
1244 growth and long-term strength in rock and cementitious material. *International Journal of*
1245 *Fracture*, *164*(1), 57–71. https://doi.org/10.1007/s10704-010-9455-z

Nara, Y., Yamanaka, H., Oe, Y., & Kaneko, K. (2013). Influence of temperature and water on subcritical crack growth parameters and long-term strength for igneous rocks. *Geophysical Journal International*, *193*(1), 47–60. https://doi.org/10.1093/gji/ggs116

Nasseri, M. H. B., Mohanty, B., & Robin, P.-Y. F. (2005). Characterization of microstructures and fracture toughness in five granitic rocks. *International Journal of Rock Mechanics and Mining Sciences*, *42*(3), 450–460. https://doi.org/10.1016/j.ijrmms.2004.11.007

Olsson, M., Niklasson, B., Wilson, L., Andersson, C., & Christiansson, R. (2004). *Aespoe HRL Experiences of blasting of the TASQ tunnel* (1402–3091; p. 74).

Ortlepp, W. D. (2000). Observation of mining-induced faults in an intact rock mass at depth. *International Journal of Rock Mechanics and Mining Sciences*, *37*(1), 423–436. https://doi.org/10.1016/S1365-1609(99)00117-3

Paraskevopoulou, C., Perras, M., Diederichs, M., Amann, F., Loew, S., Lam, T., & Jensen, M. (2016). The three stages of stress relaxation—Observations for the time-dependent behaviour of brittle rocks based on laboratory testing. *Engineering Geology*, *216*. https://doi.org/10.1016/j.enggeo.2016.11.010

Paraskevopoulou, C., Perras, M., Diederichs, M., Loew, S., Lam, T., & Jensen, M. (2018). Time-Dependent Behaviour of Brittle Rocks Based on Static Load Laboratory Tests. *Geotechnical and Geological Engineering*, *36*(1), 337–376. https://doi.org/10.1007/s10706-017-0331-8

Parasnis, D. S. (1988). Reciprocity theorems in geoelectric and geoelectromagnetic work. *Geoexploration*, *25*(3), 177–198. https://doi.org/10.1016/0016-7142(88)90014-2

Peng, S. D. (1971). Stresses within elastic circular cylinders loaded uniaxially and triaxially. *International Journal of Rock Mechanics and Mining Sciences & Geomechanics Abstracts*, *8*(5), 399–432. https://doi.org/10.1016/1365-1609(71)90009-8

Peng, S., & Johnson, A. M. (1972). Crack growth and faulting in cylindrical specimens of chelmsford granite. *International Journal of Rock Mechanics and Mining Sciences & Geomechanics Abstracts*, *9*(1), 37–86. https://doi.org/10.1016/0148-9062(72)90050-2

Perras, M. A., & Diederichs, M. S. (2016). Predicting excavation damage zone depths in brittle rocks. *Journal of Rock Mechanics and Geotechnical Engineering*, *8*(1), 60–74. https://doi.org/10.1016/j.jrmge.2015.11.004

Perras, M. A., Golabchi, Y., Bahrani, N., Hamdi, P., & Amann, F. (2024, June 23). *Intact Rock Properties of the Rotondo Granite for the PRECODE Project in the BedrettoLab*. 58th U.S. Rock Mechanics/Geomechanics Symposium. https://doi.org/10.56952/ARMA-2024-0438

Potyondy, D. O., & Cundall, P. A. (2004). A bonded-particle model for rock. *International Journal of Rock Mechanics and Mining Sciences, Rock Mechanics Results from the Underground Research Laboratory, Canada*, *41*(8), 1329–1364. https://doi.org/10.1016/j.ijrmms.2004.09.011

Potyondy, D. O., & Fu, W. (2026, June 21). *Simulating Spalling with Bonded-Particle Models*. 60th U.S. Rock Mechanics/Geomechanics Symposium. https://doi.org/10.56952/ARMA-2026-0629

Potyondy, D., Vatcher, J., & Emam, S. (2020). *Modeling of spalling with PFC3D: a quantitative assessment. Technical report for Svensk Kärnbränslehantering, AB (SKB)*.

Rasmussen, L. L., & Min, K.-B. (2024). Hybrid lattice/discrete element analysis of spalling failure in rock tunnels. *Tunnelling and Underground Space Technology*, *153*, 106034. https://doi.org/10.1016/j.tust.2024.106034

Rast, M. (2020). *Geology, Geochronology and Rock Magnetics Along Bedretto Tunnel (Gotthard Massif, Central Alps) and Numerical Modelling of Quartz-Biotite Aggregates* [Master Thesis, ETH Zurich]. https://doi.org/10.3929/ethz-b-000454117

Read, R. S. (2004). 20 years of excavation response studies at AECL's Underground Research Laboratory. *International Journal of Rock Mechanics and Mining Sciences, Rock Mechanics Results from the Underground Research Laboratory, Canada*, *41*(8), 1251–1275. https://doi.org/10.1016/j.ijrmms.2004.09.012

1299 Reches, Z., & Lockner, D. A. (1994). Nucleation and growth of faults in brittle rocks. *Journal of*
1300 *Geophysical Research: Solid Earth*, *99*(B9), 18159–18173.
1301 https://doi.org/10.1029/94JB00115
1302 Renard, F., McBeck, J., Kandula, N., Cordonnier, B., Meakin, P., & Ben-Zion, Y. (2019). Volumetric
1303 and shear processes in crystalline rock approaching faulting. *Proceedings of the National*
1304 *Academy of Sciences*, *116*(33), 16234–16239. https://doi.org/10.1073/pnas.1902994116
1305 Rógenes, E., Gomes, A. dos S., Farias, M. M. de, Fávero Neto, A. H., Vinueza, G., & Rasmussen, L.
1306 L. (2024). The impact of discontinuities on spalling failure in excavations under high-
1307 stress conditions. *Computers and Geotechnics*, *175*, 106667.
1308 https://doi.org/10.1016/j.compgeo.2024.106667
1309 Rutqvist, J., Börgesson, L., Chijimatsu, M., Hernelind, J., Jing, L., Kobayashi, A., & Nguyen, S.
1310 (2009). Modeling of damage, permeability changes and pressure responses during
1311 excavation of the TSX tunnel in granitic rock at URL, Canada. *Environmental Geology*,
1312 *57*(6), 1263–1274. https://doi.org/10.1007/s00254-008-1515-6
1313 Salazar, A. V., Selvadurai, P. A., Niu, Z., Bianchi, P., Rabaiotti, C., Madonna, C., Wiemer, S., &
1314 Germanovich, L. N. (2022, June 26). *Insights into Triaxial Testing Using Coupled Acoustic*
1315 *Emission and Distributed Optical Fiber Strain Measurements*. 56th U.S. Rock
1316 Mechanics/Geomechanics Symposium. https://doi.org/10.56952/ARMA-2022-0706
1317 Salazar Vásquez, A. F., Selvadurai, P. A., Bianchi, P., Madonna, C., Germanovich, L. N., Puzrin, A.
1318 M., Wiemer, S., Giardini, D., & Rabaiotti, C. (2024). Aseismic strain localization prior to
1319 failure and associated seismicity in crystalline rock. *Scientific Reports*, *14*(1), 29954.
1320 https://doi.org/10.1038/s41598-024-75942-9
1321 Sanipour, S. (2021). *Simulation of Brittle Rock Failure Using 2D Continuum-Based Voronoi*
1322 *Tessellated Models*. https://DalSpace.library.dal.ca//handle/10222/80656
1323 Sanipour, S., Bahrani, N., & Corkum, A. (2022). Simulation of Brittle Failure Around Canada's
1324 Mine-By Experiment Tunnel Using 2D Continuum-Based Voronoi Tessellated Models.

Rock Mechanics and Rock Engineering, *55*(10), 6387–6408. https://doi.org/10.1007/s00603-022-02969-7

Schmidtke, R. H., & Lajtai, E. Z. (1985). The long-term strength of lac du bonnet granite. *International Journal of Rock Mechanics and Mining Sciences & Geomechanics Abstracts*, *22*(6), 461–465. https://doi.org/10.1016/0148-9062(85)90010-5

Scholz, C. H. (1968). Experimental study of the fracturing process in brittle rock. *Journal of Geophysical Research (1896-1977)*, *73*(4), 1447–1454. https://doi.org/10.1029/JB073i004p01447

Shakas, A., Hertrich, M., Gischig, V., Giardini, D., Meier, M.-A., Wimez, M., Vargas Meleza, L., Kövér, B., Zappone, A. S., Hamdi, P., Pfammatter, P., Ceccato, A., & Hibbard, L. (2026). *FEAR borehole trajectories: Bedretto Lab Fault Activation and Earthquake Rupture project*. http://hdl.handle.net/20.500.11850/797493

Shin, S. W., Martin, C. D., Park, E. S., & Christiansson, R. (2007, January 1). *Methodology for estimation of excavation damaged zone around tunnels in hard rock*. 1st Canada - U.S. Rock Mechanics Symposium. https://www.onepetro.org/conference-paper/ARMA-07-060?sort=&start=0&q=Methodology+for+estimation+of+excavation+damaged+zone+around+tunnels+in+hard+rock&from_year=&peer_reviewed=&published_between=&fromSearchResults=true&to_year=&rows=10#

Sibson, R. H. (1990). Conditions for fault-valve behaviour. *Geological Society, London, Special Publications*, *54*(1), 15–28. https://doi.org/10.1144/GSL.SP.1990.054.01.02

Siren, T., Kantia, P., & Rinne, M. (2015). Considerations and observations of stress-induced and construction-induced excavation damage zone in crystalline rock. *International Journal of Rock Mechanics and Mining Sciences*, *73*, 165–174. https://doi.org/10.1016/j.ijrmms.2014.11.001

SKB Report. (2011). *Long-term safety for the final repository for spent nuclear fuel at Forsmark. Main report of the SR-Site project. Updated 2015-05 – SKB.com*. https://www.skb.com/publication/2345580/

1352 Sue, C., Delacou, B., Champagnac, J.-D., Allanic, C., Tricart, P., & Burkhard, M. (2007).
1353 Extensional neotectonics around the bend of the Western/Central Alps: An overview.
1354 *International Journal of Earth Sciences*, *96*(6), 1101–1129.
1355 https://doi.org/10.1007/s00531-007-0181-3
1356 Tapponnier, P., & Brace, W. F. (1976). Development of stress-induced microcracks in Westerly
1357 Granite. *International Journal of Rock Mechanics and Mining Sciences & Geomechanics*
1358 *Abstracts*, *13*(4), 103–112. https://doi.org/10.1016/0148-9062(76)91937-9
1359 Terzaghi, K. (1962). Stability of Steep Slopes on Hard Unweathered Rock. *Géotechnique*, *12*(4),
1360 251–270. https://doi.org/10.1680/geot.1962.12.4.251
1361 Torsello, G., Hamdi, P., Amann, F., Castelli, M., & Fidelibus, C. (2026). The influence of porosity
1362 on the damage induced by freeze-thaw cycles on fracture toughness. *Engineering*
1363 *Geology*, *371*, 108891. https://doi.org/10.1016/j.enggeo.2026.108891
1364 Tsang, C.-F., Bernier, F., & Davies, C. (2005). Geohydromechanical processes in the Excavation
1365 Damaged Zone in crystalline rock, rock salt, and indurated and plastic clays—In the
1366 context of radioactive waste disposal. *International Journal of Rock Mechanics and*
1367 *Mining Sciences*, *42*(1), 109–125. https://doi.org/10.1016/j.ijrmms.2004.08.003
1368 Tso, C.-H. M., Kuras, O., Wilkinson, P. B., Uhlemann, S., Chambers, J. E., Meldrum, P. I., Graham,
1369 J., Sherlock, E. F., & Binley, A. (2017). *Improved characterisation and modelling of*
1370 *measurement errors in electrical resistivity tomography (ERT) surveys*.
1371 https://doi.org/10.1016/j.jappgeo.2017.09.009
1372 Valley, B., Suorineni, F. T., & Kaiser, P. K. (2010, June 27). *Numerical Analyses of the Effect of*
1373 *Heterogeneities On Rock Failure Process*. 44th U.S. Rock Mechanics Symposium and 5th
1374 U.S.-Canada Rock Mechanics Symposium. https://dx.doi.org/
1375 Vazaios, I., Vlachopoulos, N., & Diederichs, M. S. (2019). Mechanical analysis and interpretation
1376 of excavation damage zone formation around deep tunnels within massive rock masses
1377 using hybrid finite–discrete element approach: Case of Atomic Energy of Canada Limited

(AECL) Underground Research Laboratory (URL) test tunnel. *Canadian Geotechnical Journal*, *56*(1), 35–59. https://doi.org/10.1139/cgj-2017-0578

Wang, C., Zhao, X., Liu, J., Zhang, H., Chen, L., Ma, H., & Wang, J. (2026). Long-term creep of Beishan granite under uniaxial compression. *International Journal of Mining Science and Technology*, *36*(1), 79–93. https://doi.org/10.1016/j.ijmst.2025.10.009

Winhausen, L., Klaver, J., Schmatz, J., Desbois, G., Urai, J. L., Amann, F., & Nussbaum, C. (2021). Micromechanisms leading to shear failure of Opalinus Clay in a triaxial test: A high-resolution BIB–SEM study. *Solid Earth*, *12*(9), 2109–2126. https://doi.org/10.5194/se-12-2109-2021

Wu, R., Selvadurai, P. A., Li, Y., Sun, Y., Leith, K., & Loew, S. (2023). Laboratory acousto-mechanical study into moisture-induced changes of elastic properties in intact granite. *International Journal of Rock Mechanics and Mining Sciences*, *170*, 105511. https://doi.org/10.1016/j.ijrmms.2023.105511

Yang, Z., Yehya, A., Iwalewa, T. M., & Rice, J. R. (2021). Effect of Permeability Evolution in Fault Damage Zones on Earthquake Recurrence. *Journal of Geophysical Research: Solid Earth*, *126*(9), e2021JB021787. https://doi.org/10.1029/2021JB021787